SUPPLEMENTAL MATERIALS

ASCE *Journal of Structural Engineering*

Validation of Numerical Modeling Techniques for Unbonded Post-Tensioned Beams under Low-Velocity Impact

Andrew Nghiem and Thomas H.-K. Kang

DOI: 10.1061/(ASCE)ST.1943-541X.0003373

www.ascelibrary.org

APPENDIX S1

Experimental Testing Details

The design cross-section used for this study was comprised of a 220 x 400 mm section with reinforcement provided as shown in **Fig. 4** (illustrated again here for reference). The experimental test set-up and instrumentation is shown **Fig. S1**, displacement transducers (D1 to D5) were placed as given in the figure.

Design and testing parameters can be seen in **Table A1**. Static shear and flexural capacities were calculated per the ACI 318-19 (ACI, 2019) design code following sections 20 and 22. Flexural resistances of PT members were evaluated per Haralji (2006), for determining effective prestress at the ultimate stage. Accordingly, Equations 22.5.3.6.1c and 22.5.6.3.2 were used to calculate the shear contribution of the concrete for shear strength of RC and unbonded PT-RC members, respectively. Shear contribution of the transverse steel reinforcement was provided per Equation 22.5.8.5.3. For shear series beams, SL and SM, resistance due to transverse reinforcement was not taken into consideration.

The designation of the specimen is given by the ID tag, F/S-L/M/H-RC/PT#, where the F or S represents flexural or shear specimens and the second letter denotes the drop weight velocity (L=lower, M=medium, H=high). This was then followed by the specific beam type, RC or PT, representing conventional RC and PT-RC type specimens, accordingly. For PT-RC beams, the numerical value to the right represents the measured PT force in kN in a single PT bar. For example, the specimen SLPT120 refers to a shear-critical PT specimen that was post tensioned with a measured value of 120 kN per PT bar, and tested at a low drop height of 1.75 m.

APPENDIX S2

Additional Modeling Details

Additional modeling details are given here. **Fig. S2** shows a diagram of the support system as modeled in LS-DYNA. As noted, cross plates were tied through use of rigid beam elements creating a pseudo box for placement of the concrete beam member using keyword "TIED_NODES_TO_SURFACE_OFFSET" to perfectly connect the two elements. The bottom cross plates were then similarly tied to cylindrical elements where boundary conditions were applied (using keyword "TIED_SURFACE_TO_SURFACE_OFFSET), defined by allowance for rotation at the left support and rotation plus movement along the horizontal axis at the right support. **Fig. S3** shows the resulting support conditions of the NLFEDA model.

The cross-section used for modeling of the concrete mesh is shown in **Fig. S4**. LS-DYNA default Type 1 solid elements were used and formed using the coarse and fine arrangement at the left and right, respectively. Note the circular void which was used as the PT duct for the unbonded tendon. The cross-section was repeated at 20 and 10 mm lengths to develop the member elevation shown in **Fig. S5** for coarse and fine members, given at the top and bottom, respectively.

The general behavior of the material models used for the steel reinforcements are given in **Fig. S7**, where l and l_0 are the undeformed and deformed lengths of uniaxial tension.

APPENDIX S3

Comparison of NLFEDA Modeling of Shear and Flexural Members with Experimental Results

Comparison of all obtained NLFEDA time histories with the respective experimental test data is given in **Fig. 8**, **11** and **S8** to **C50**. These include: (1) progression of the damage from time of impact toward the peak response of member deformation (approximately t = 15 *ms*); (2) time history of all force related data (impact, reaction, and PT forces); then (3) followed by comparison of the NLFEDA member deformation with that as obtained in lab (displacement transducers at locations D1 to D5, per **Fig. S1**).

REFERENCES

ACI Committee 318, "Building code requirements for structural concrete (ACI 318-19) and commentary (ACI 318R-19)," American Concrete Institute, Farmington Hills, MI, 2019.

Haraji, M., "On the stress in unbonded tendons at ultimate: critical assessment and proposed changes," *ACI Struct. J.*, **103**(6), 2006.

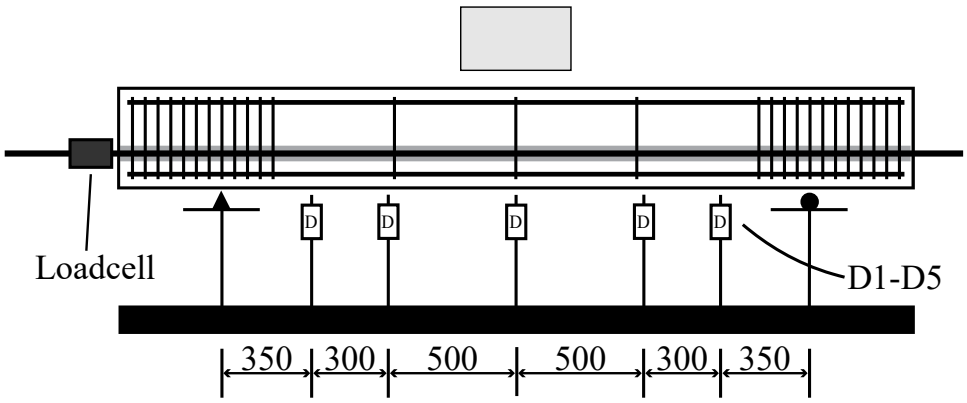

Fig. S1 – Experimental testing set-up (units: mm)

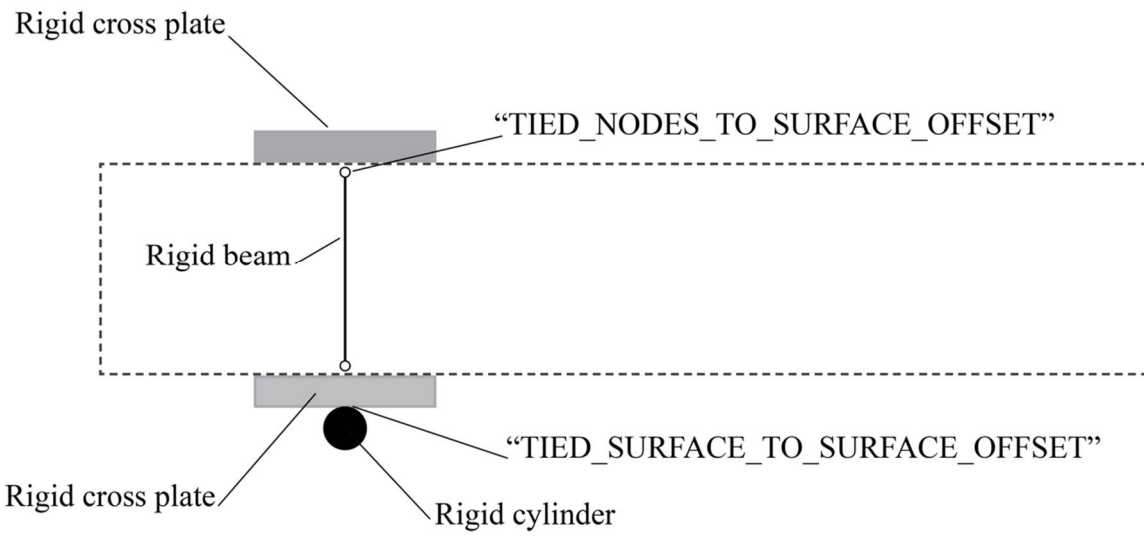

Fig. S2 – Modeling and specific keywords of the drop weight support system

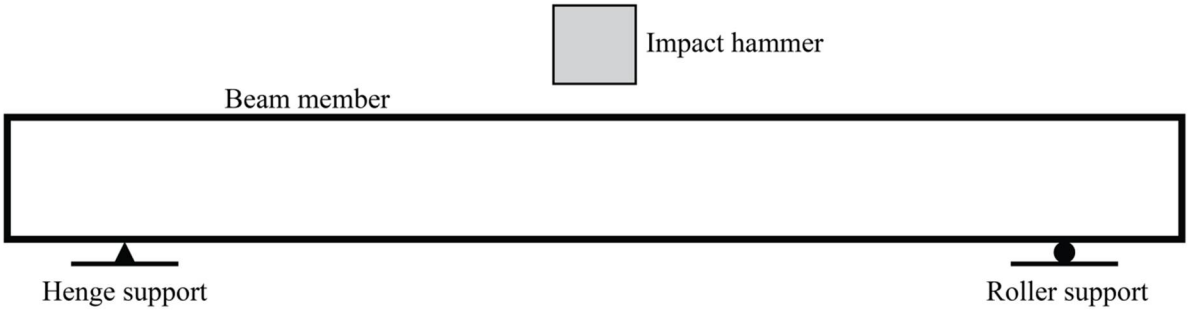

Fig. S3 – Modeled support conditions of the NLFEDA model

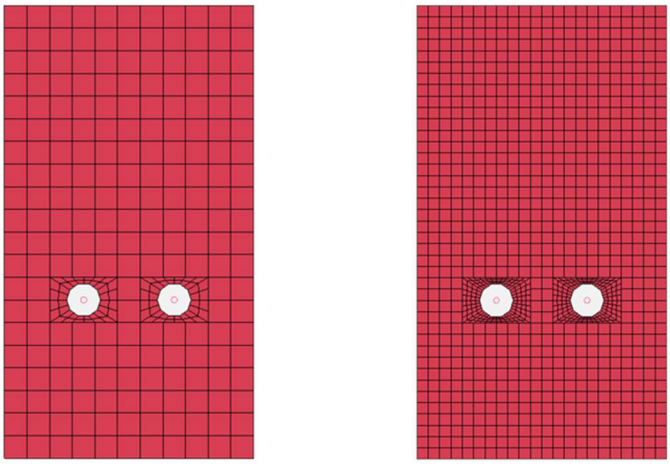

Fig. S4 – NLFEDA model cross-section for coarse and fine (20 & 10 mm) elements, left and right, respectively

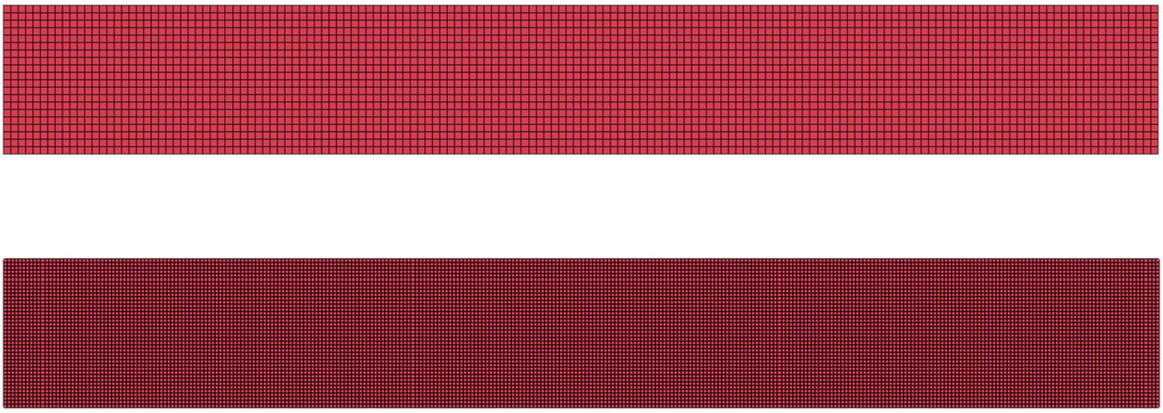

Fig. S5 – NLFEDA model elevation for coarse and fine (20 & 10 mm) elements, top and bottom, respectively

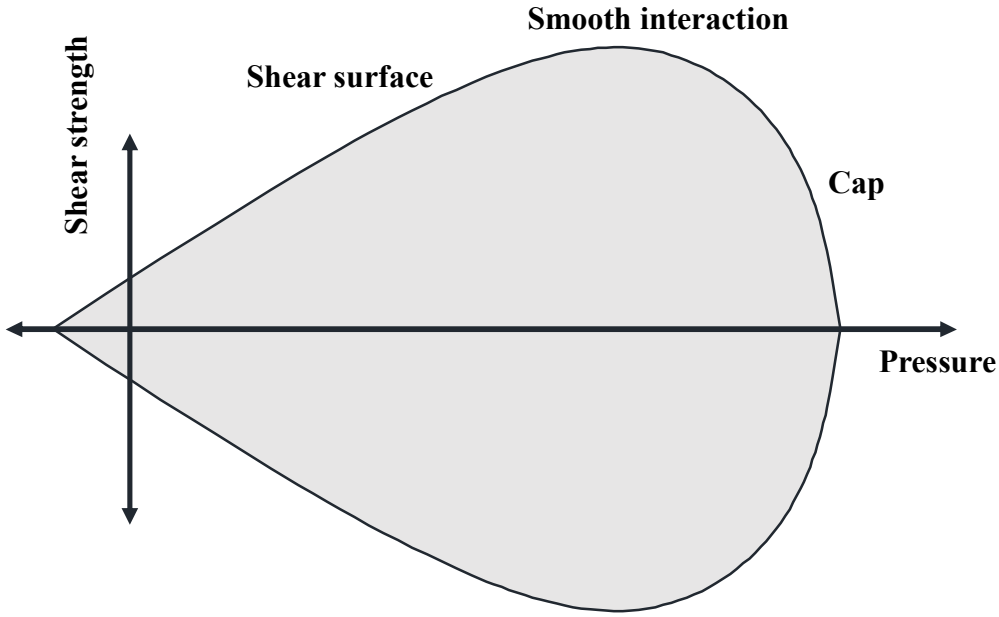

Fig. S6 – General shape of concrete material CSCM (MAT_159).

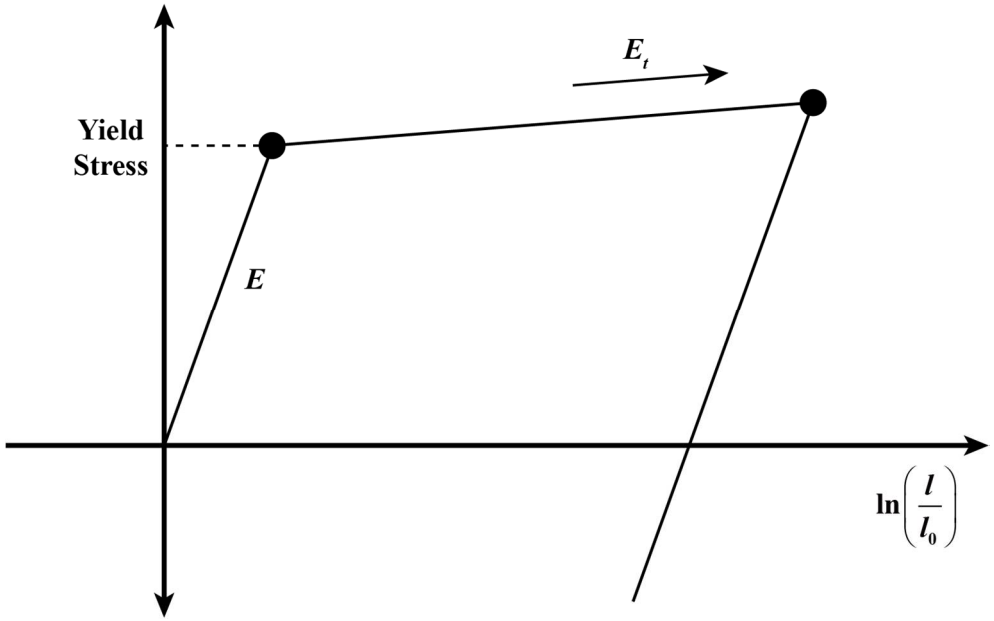

Fig. S7 – General behavior of MAT_003 and MAT_100 (PLASTIC_KINEMATIC and SPOTWELD).

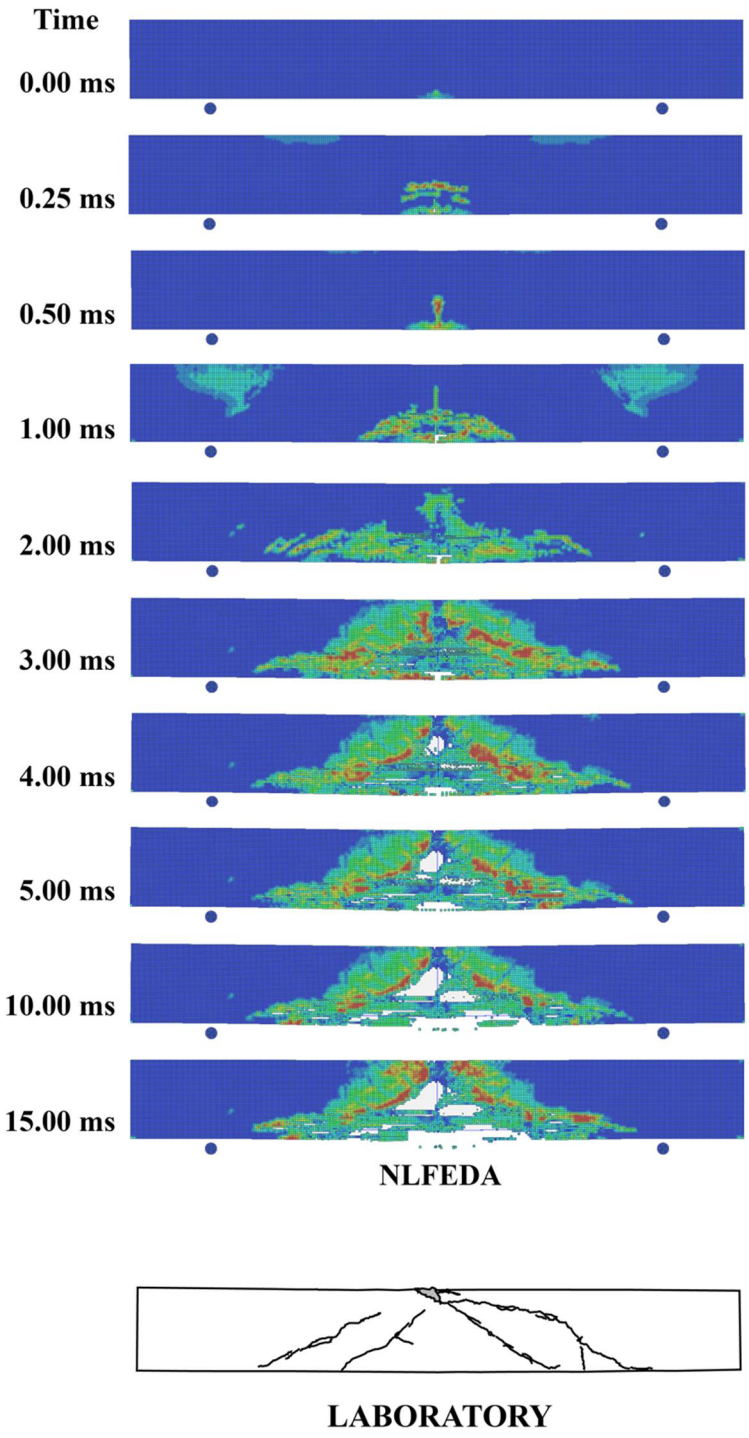

Fig. S8 – Progressive damage of SLPT120(N)

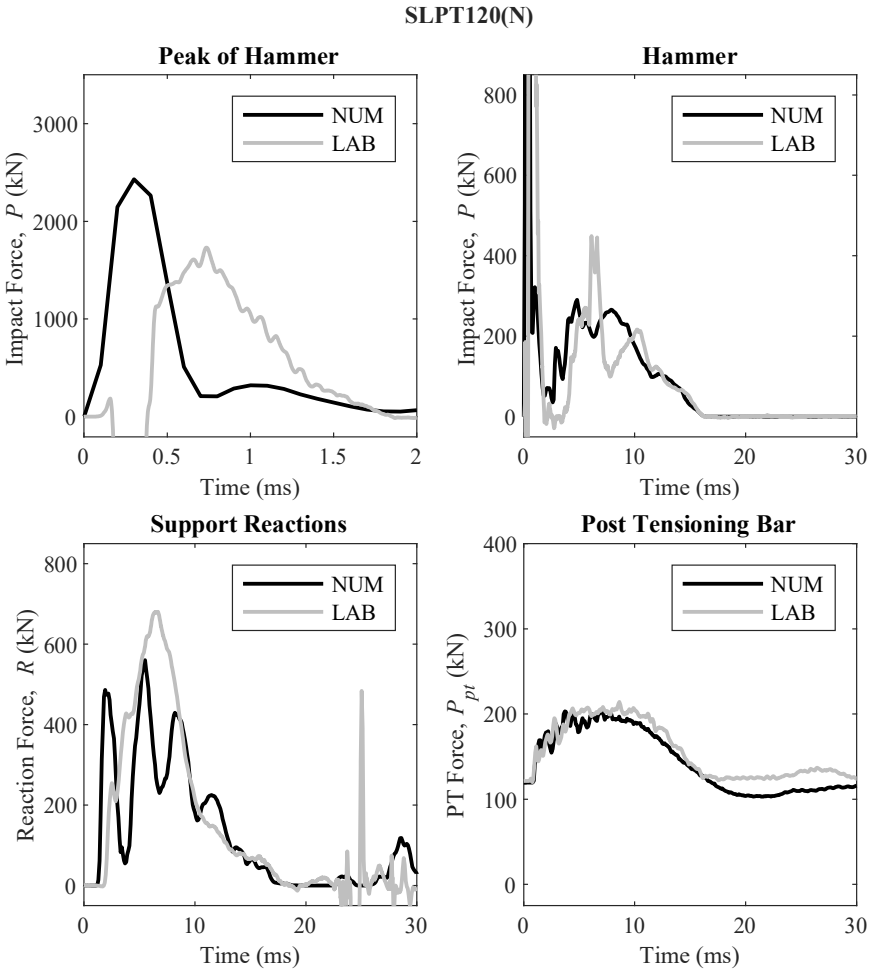

Fig. S9 – Comparison of time histories (forces) of NLFEDA modeling with laboratory results for SLPT120(N)

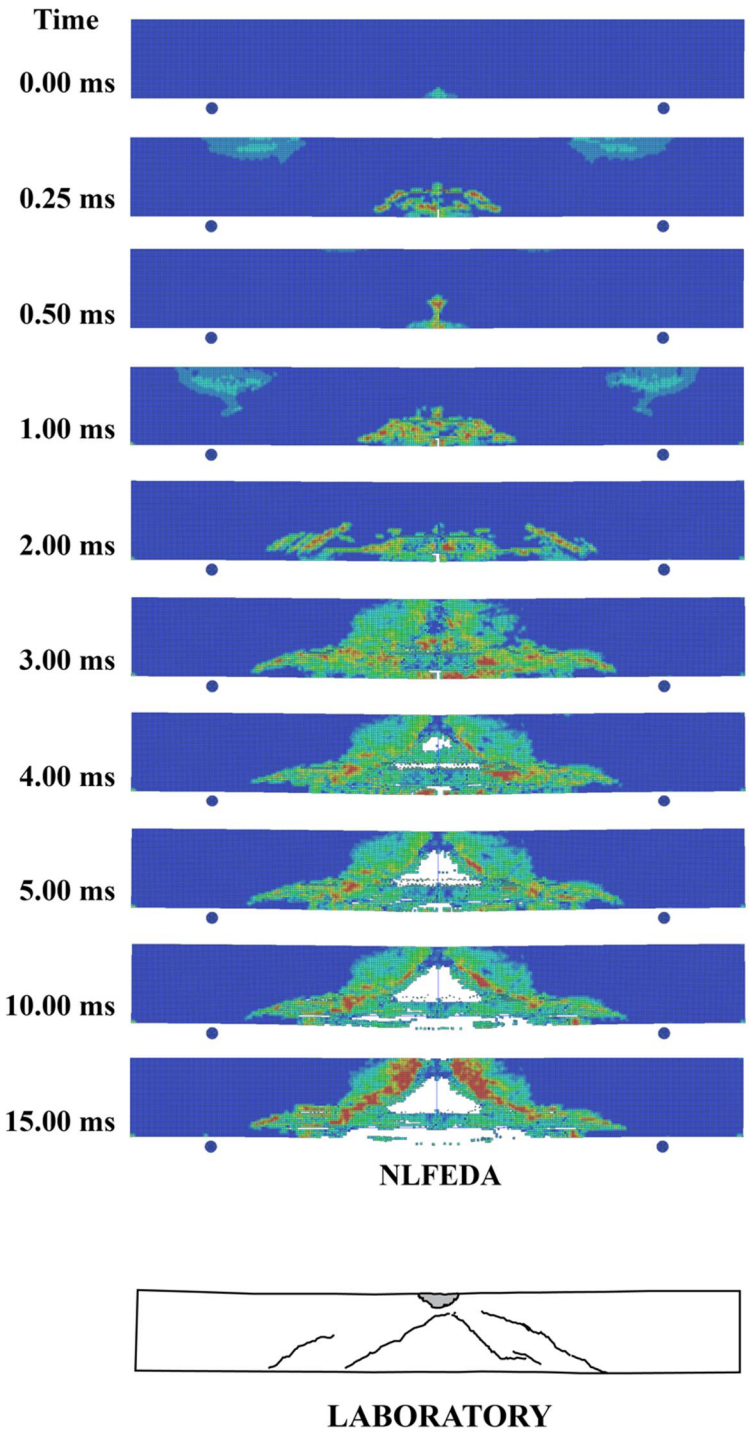

Fig. S10 – Progressive damage of SLPT172(N)

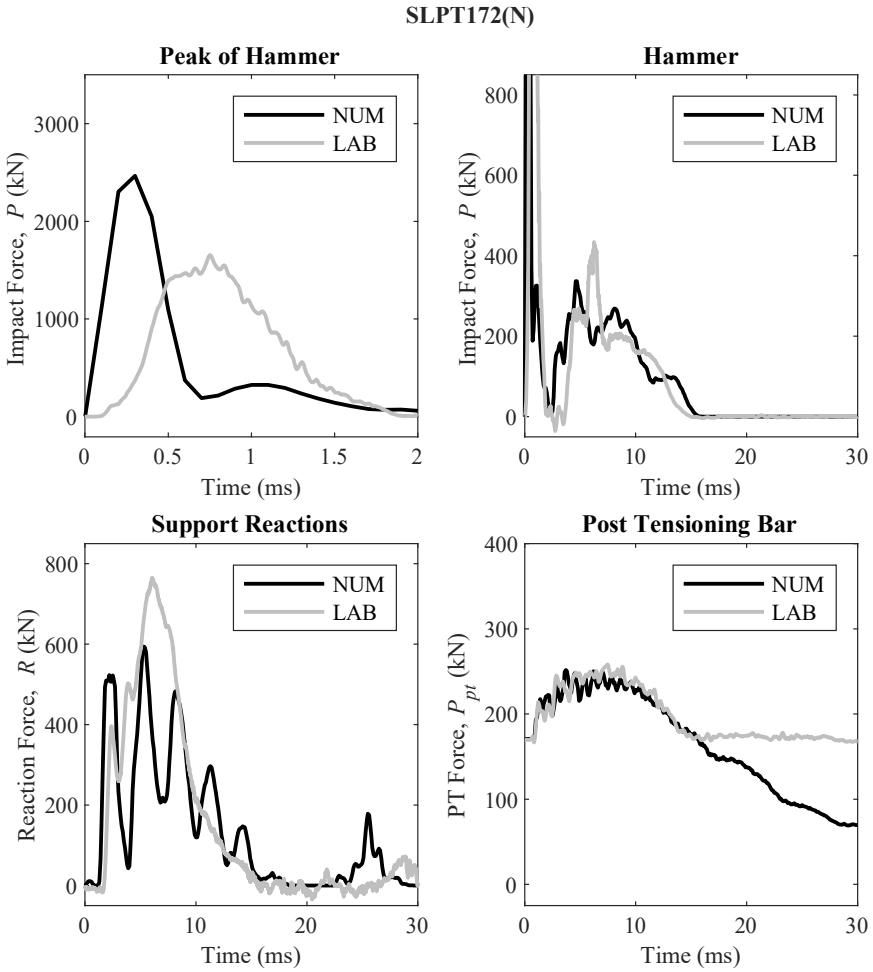

Fig. S11 – Comparison of time histories (forces) of NLFEDA modeling with laboratory results for SLPT172(N)

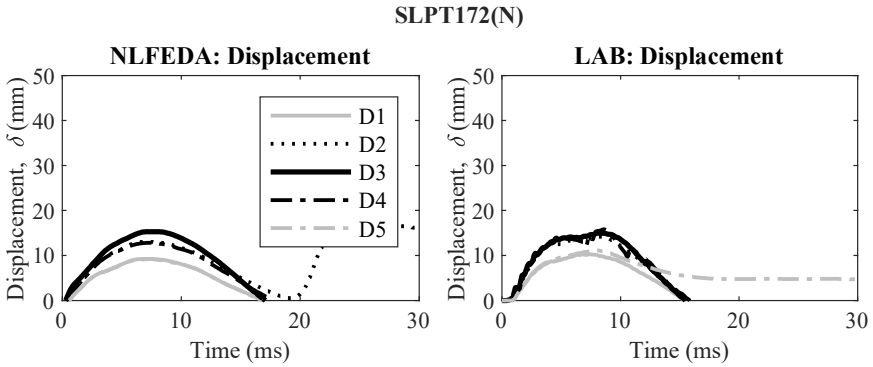

Fig. S12 – Comparison of displacement time histories of NLFEDA modeling with laboratory results for SLPT172(N)

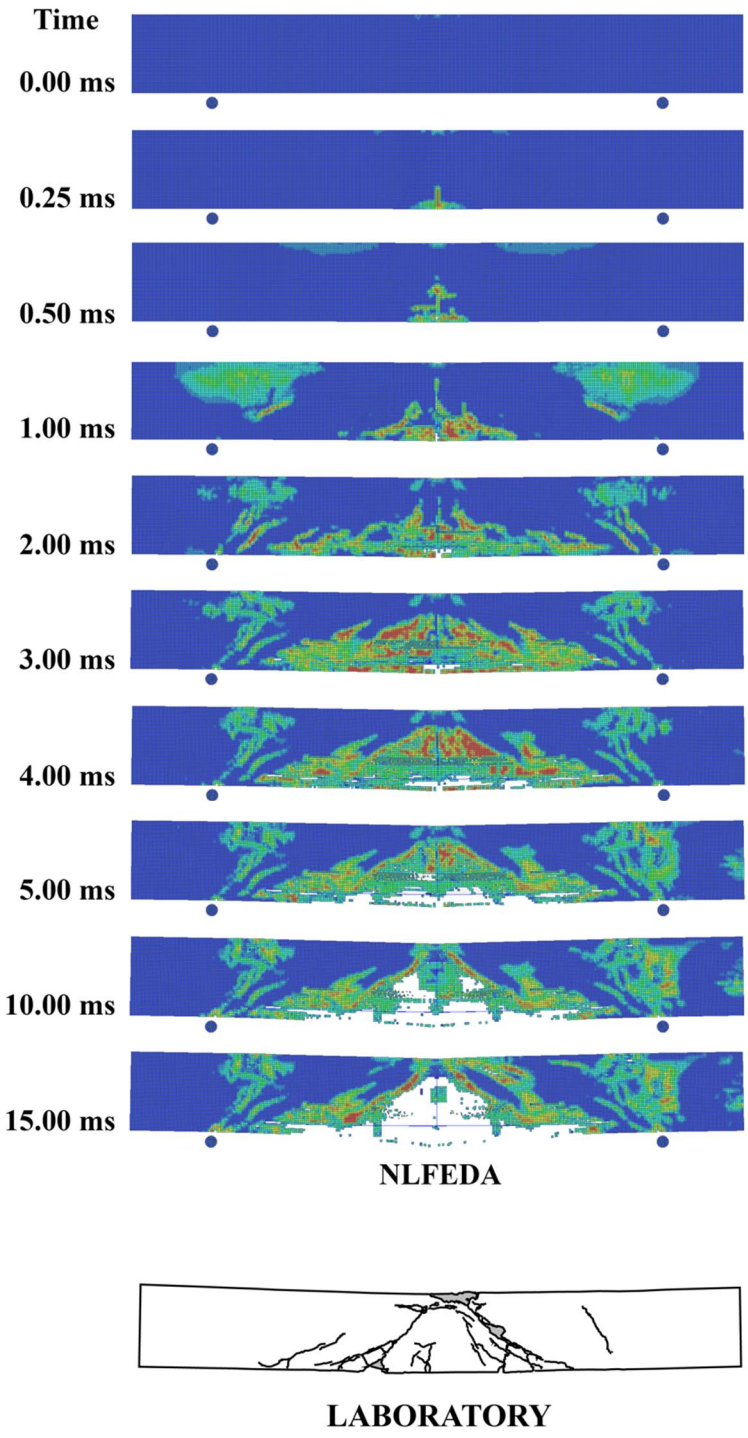

Fig. S13 – Progressive damage of SMRC(N)

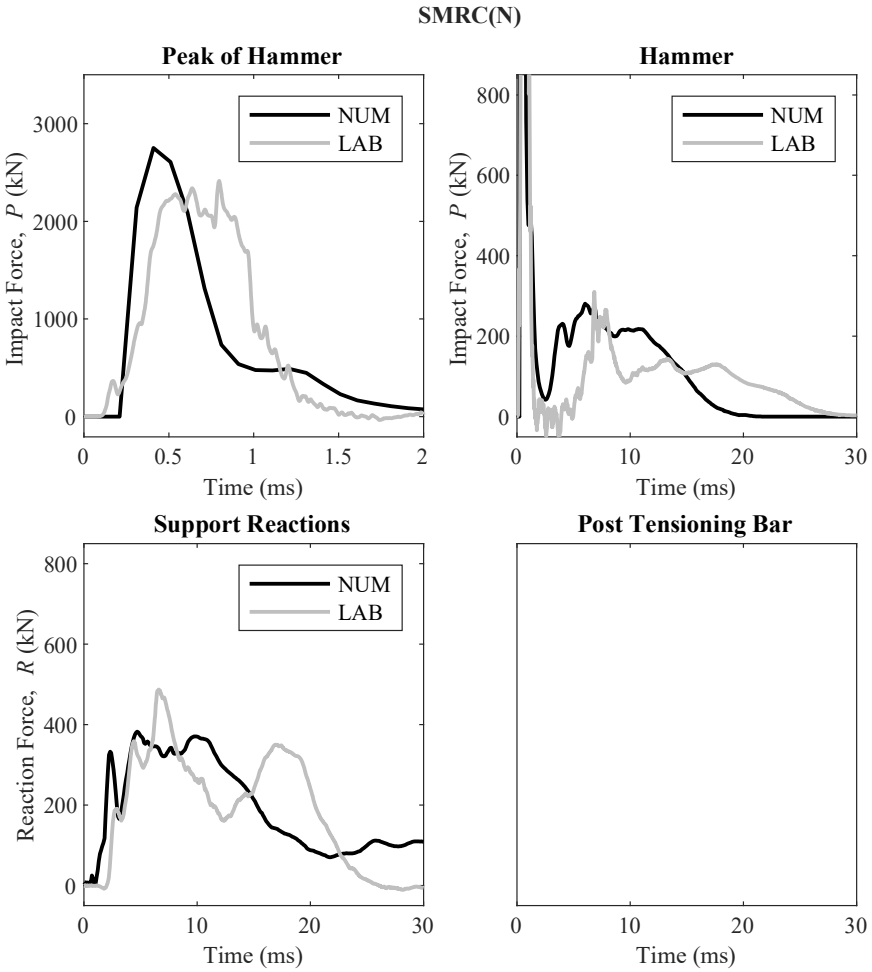

Fig. S14 – Comparison of time histories (forces) of NLFEDA modeling with laboratory results for SMRC(N)

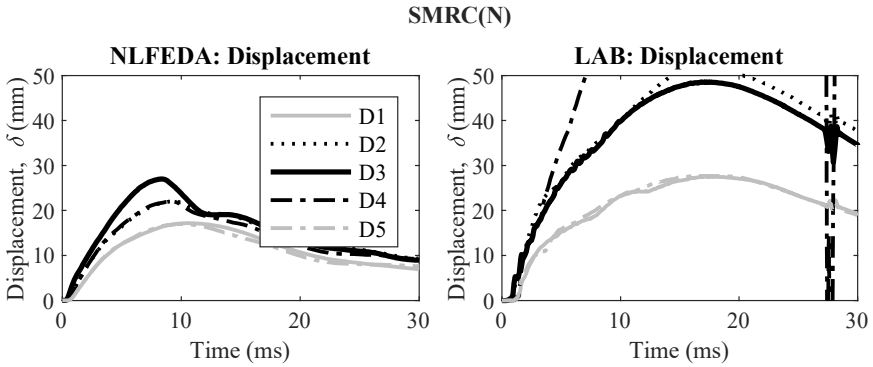

Fig. CS15 – Comparison of displacement time histories of NLFEDA modeling with laboratory results for SMRC(N)

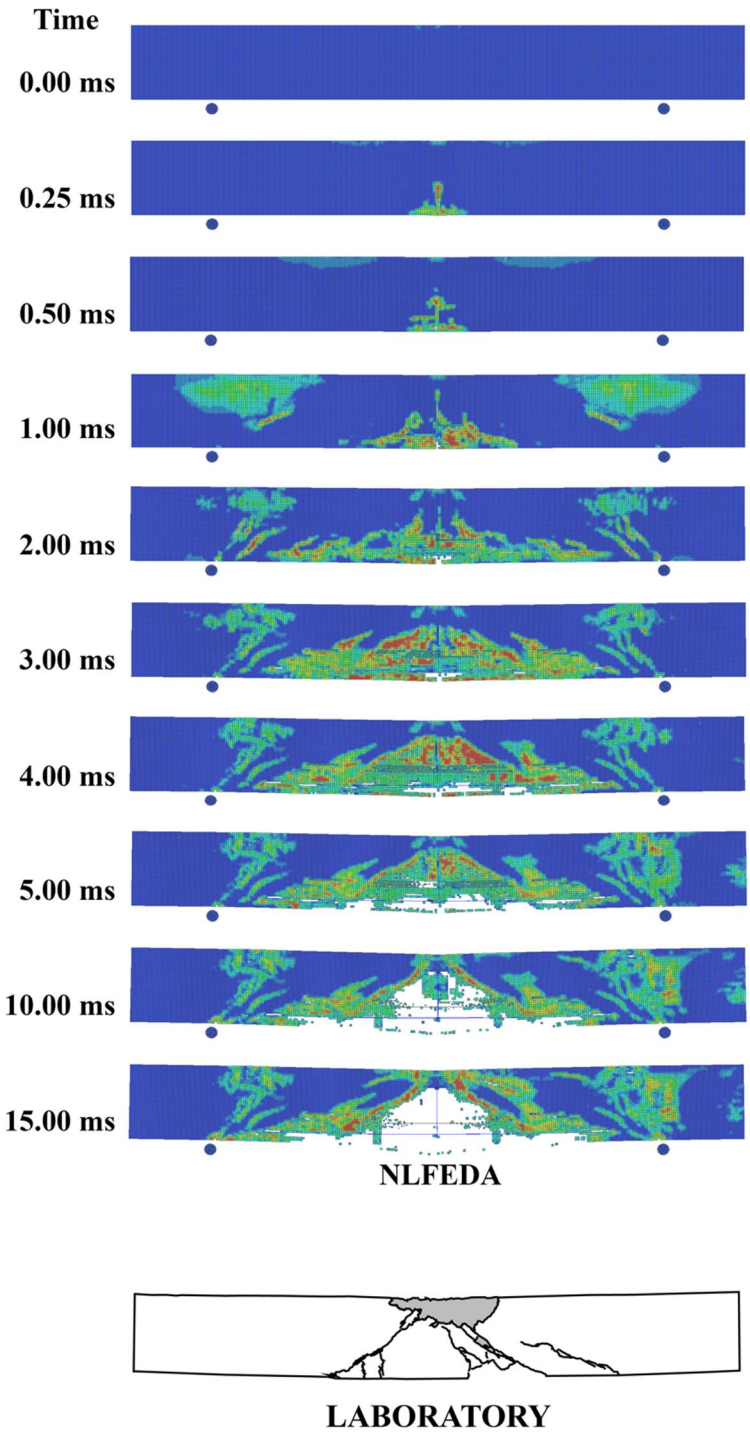

Fig. S16 – Progressive damage of SMP0(N)

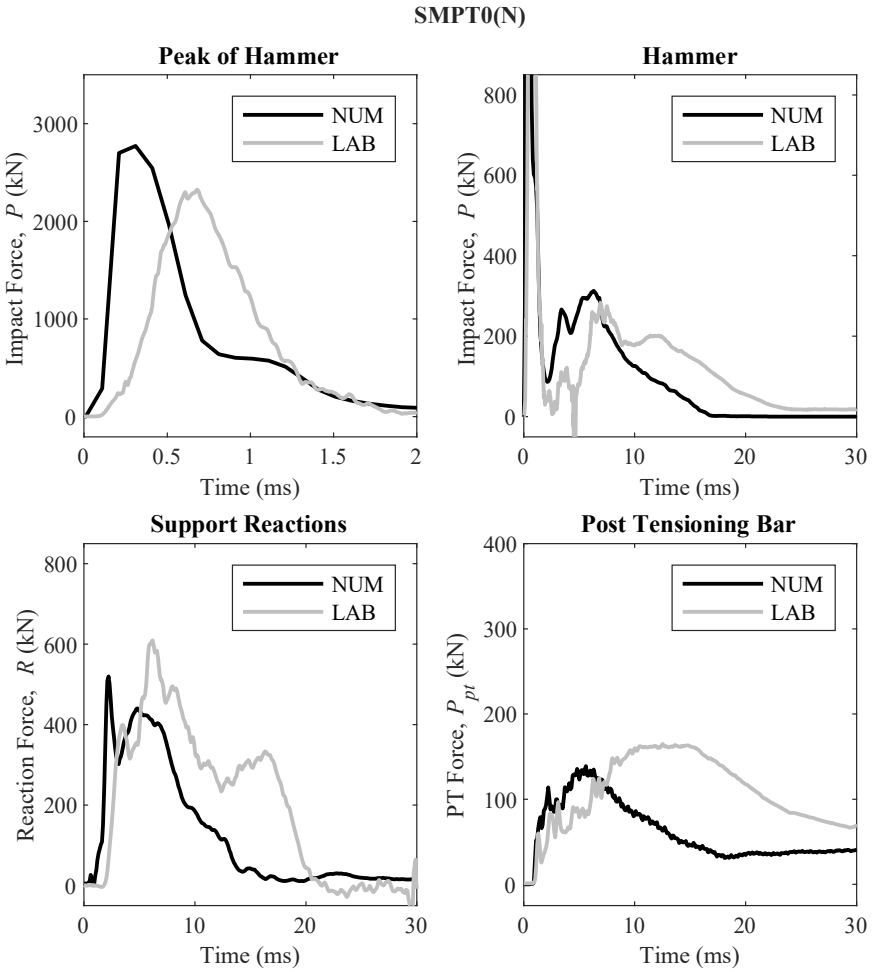

Fig. S17 – Comparison of time histories (forces) of NLFEDA modeling with laboratory results for SMPT0(N)

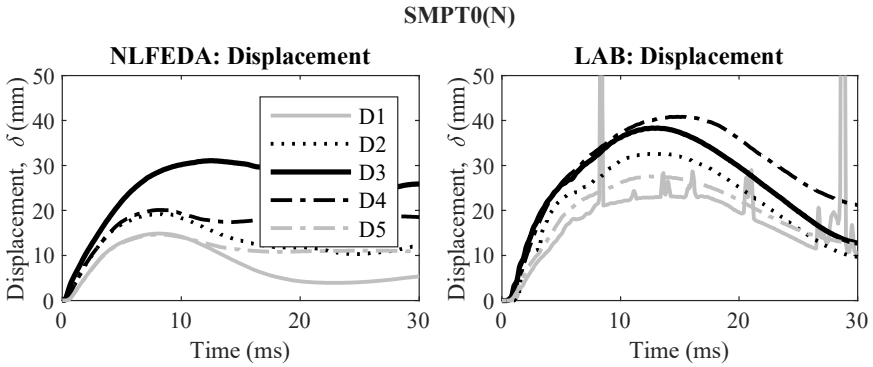

Fig. S18 – Comparison of displacement time histories of NLFEDA modeling with laboratory results for SMPT0(N)

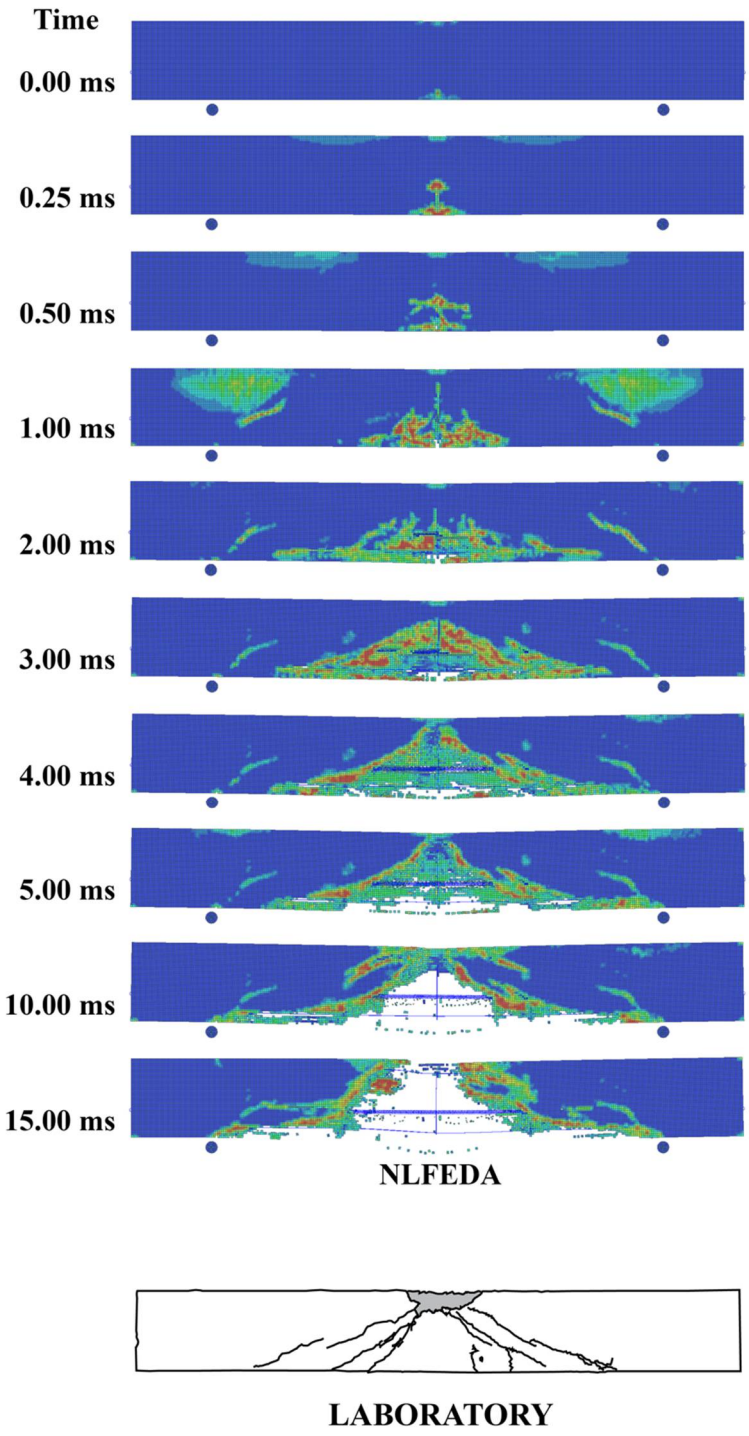

Fig. S19 – Progressive damage of SMP57(N)

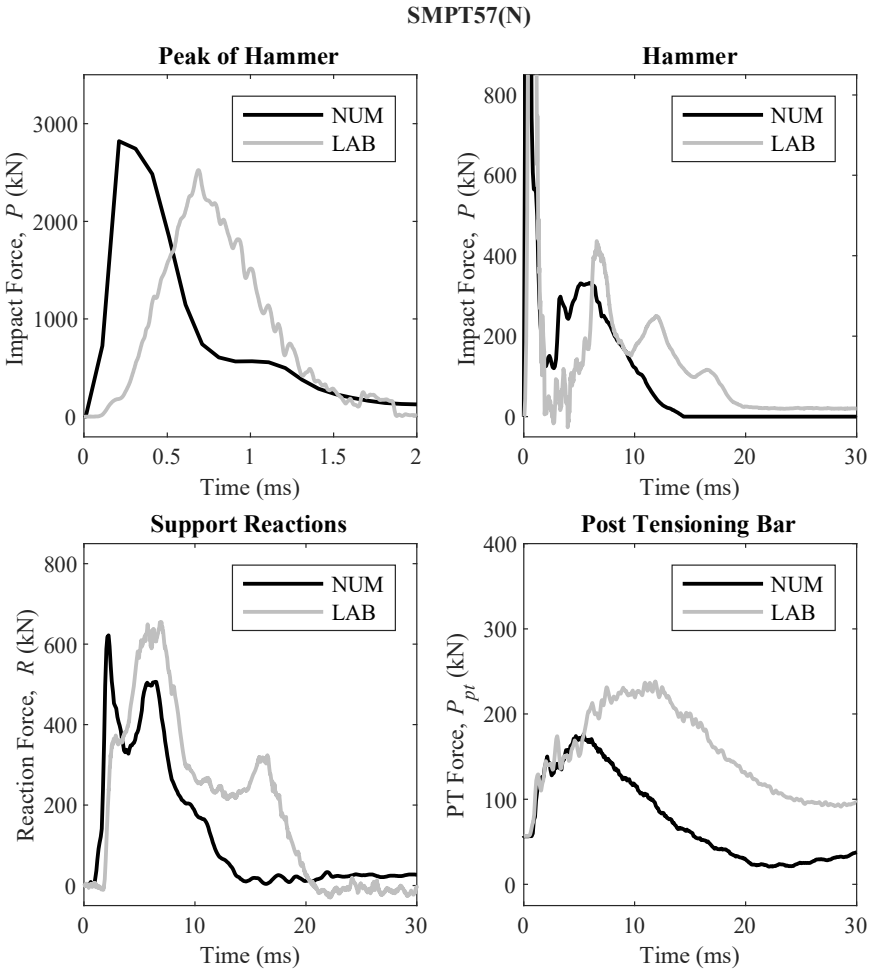

Fig. S20 – Comparison of time histories (forces) of NLFEDA modeling with laboratory results for SMPT57(N)

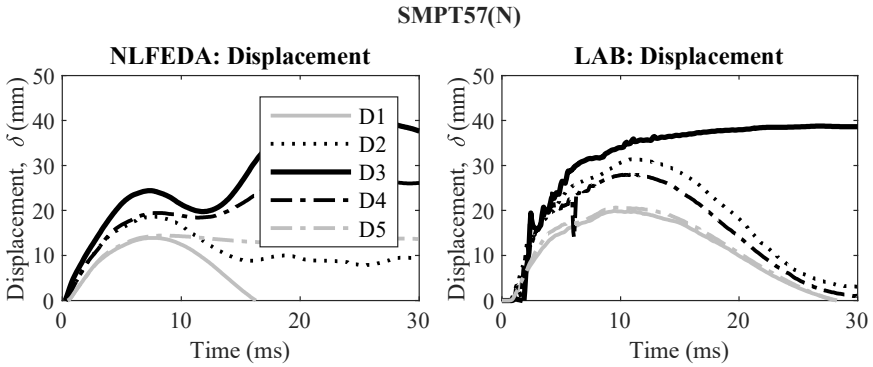

Fig. S21 – Comparison of displacement time histories of NLFEDA modeling with laboratory results for SMPT57(N)

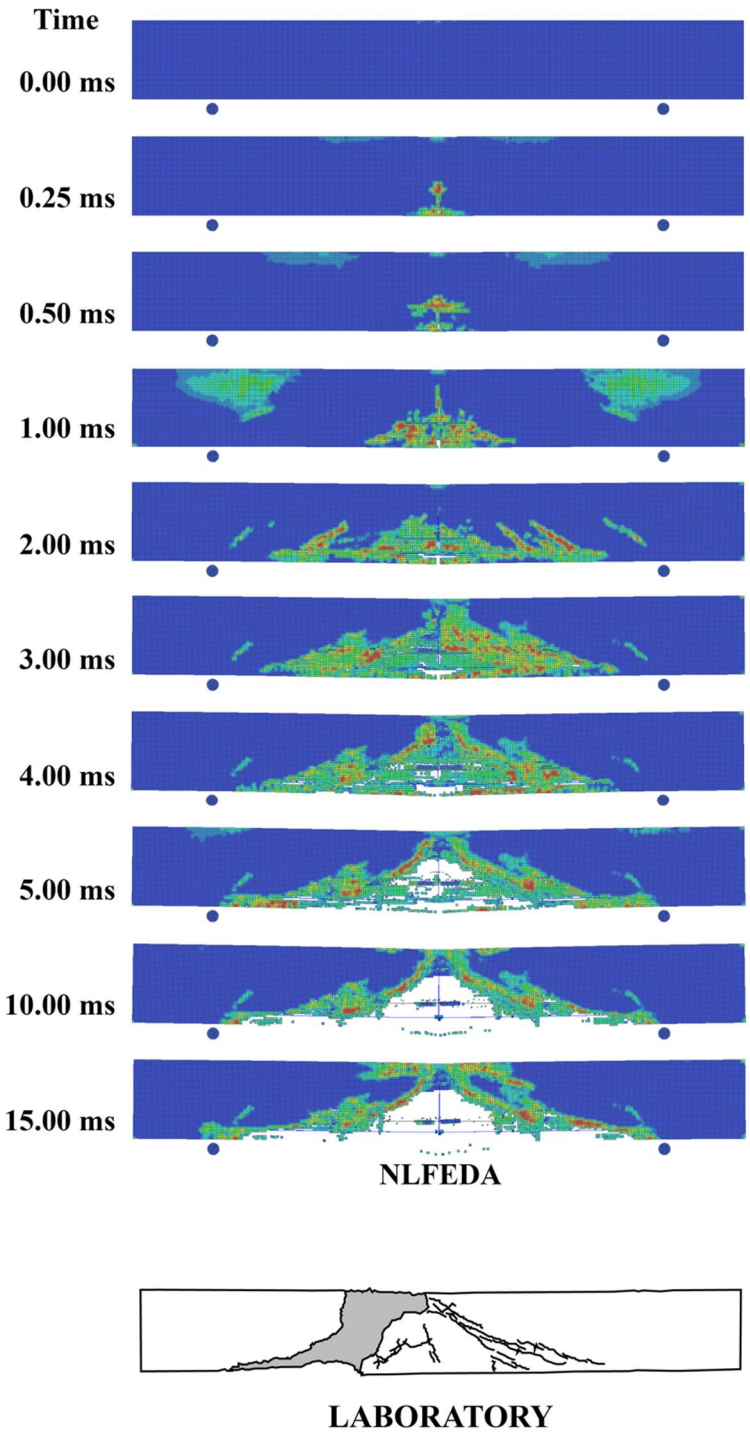

Fig. S22 – Progressive damage of SMPT118(N)

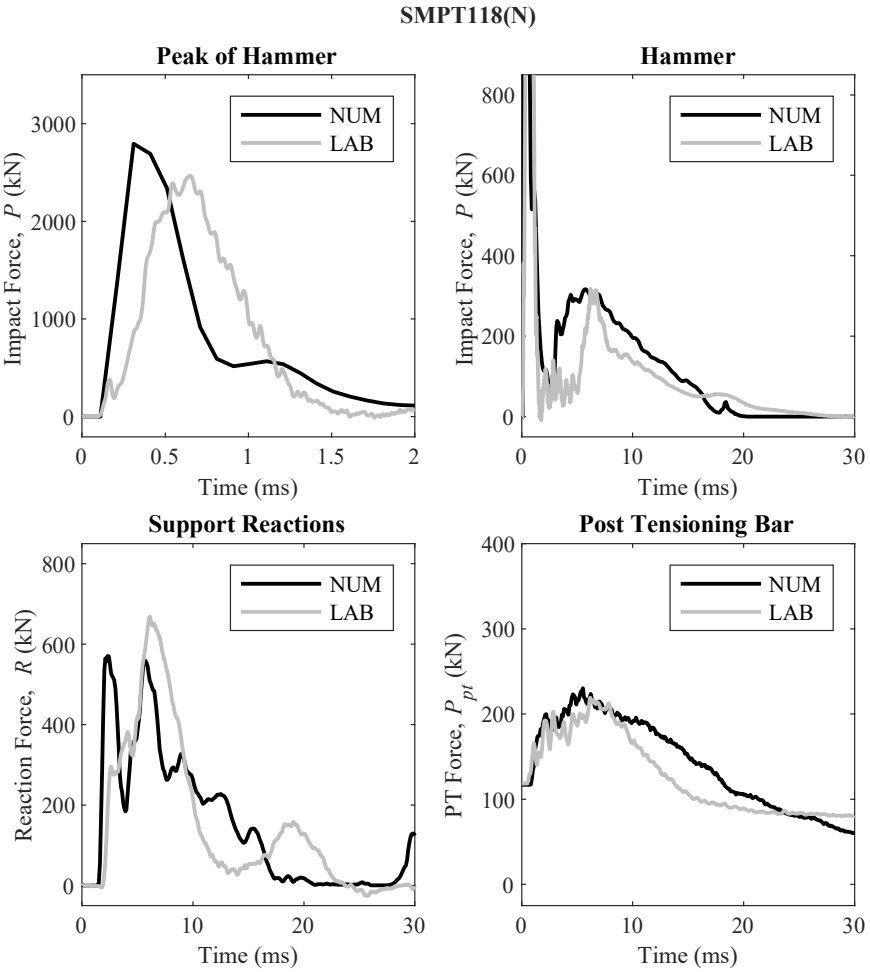

Fig. S23 – Comparison of time histories (forces) of NLFEDA modeling with laboratory results for SMPT118(N)

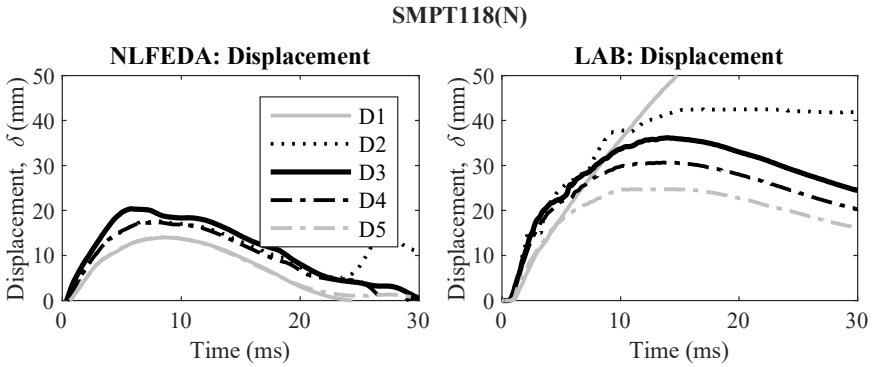

Fig. S24 – Comparison of displacement time histories of NLFEDA modeling with laboratory results for SMPT118(N)

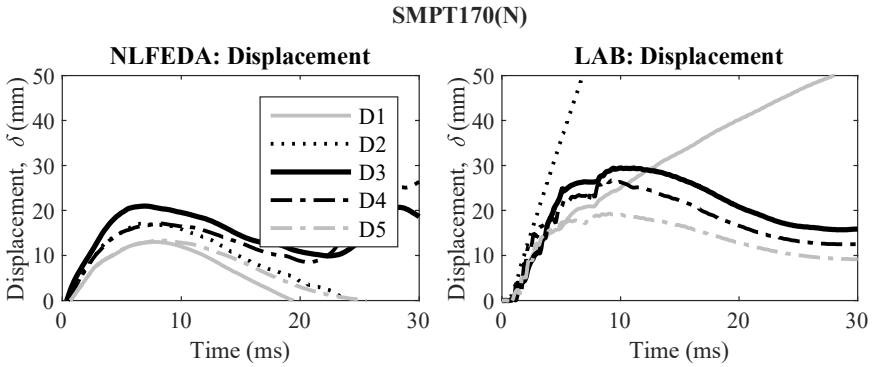

Fig. S25 – Comparison of displacement time histories of NLFEDA modeling with laboratory results for SMPT170(N)

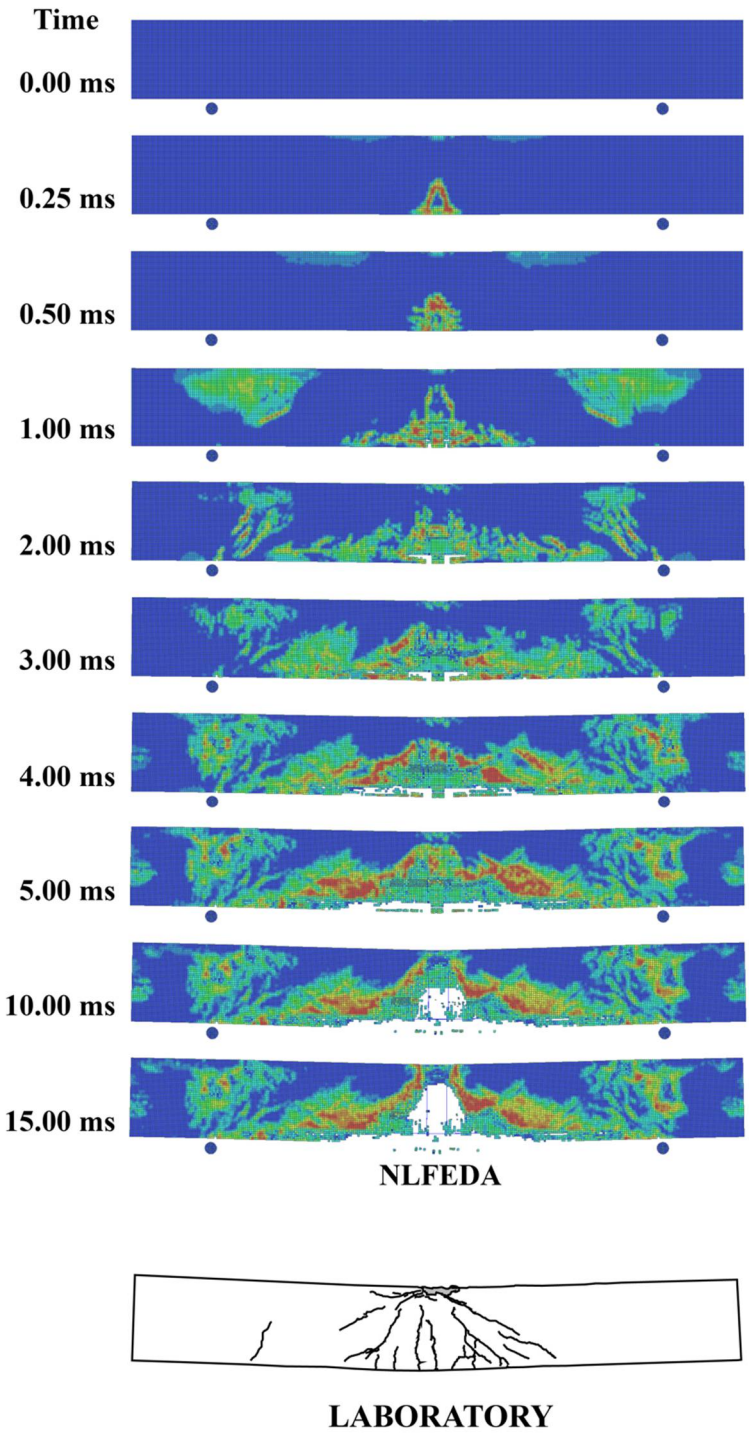

Fig. S26 – Progressive damage of FMRC(N)

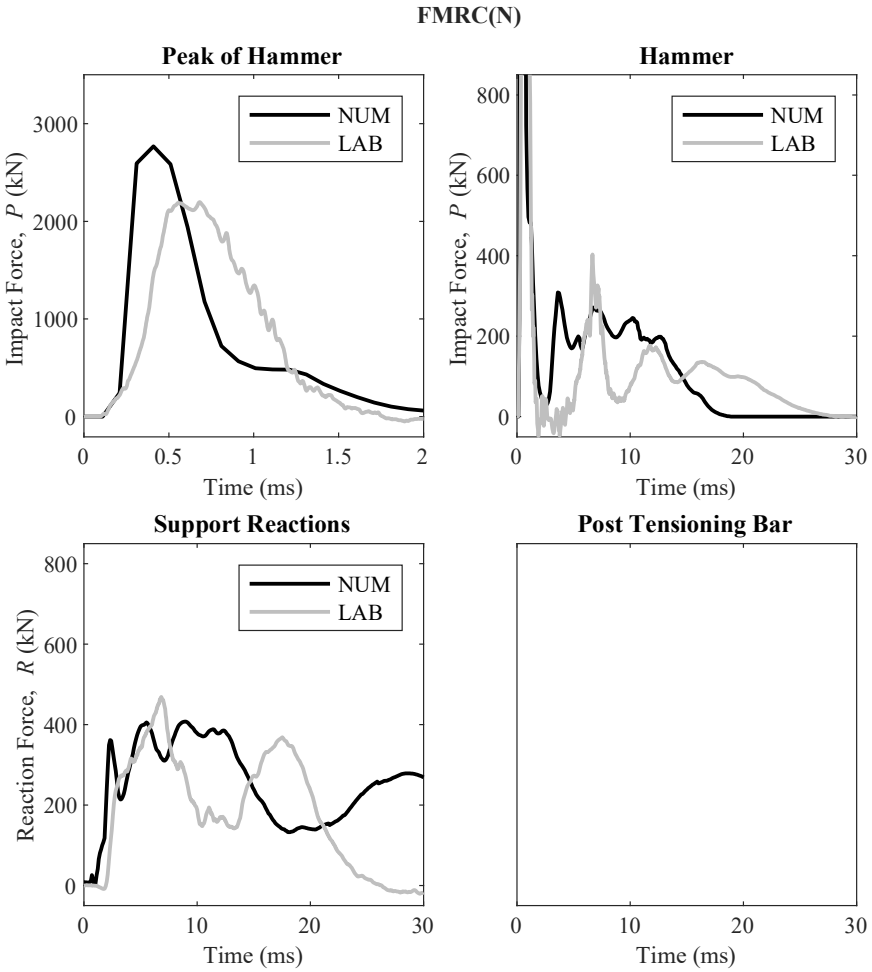

Fig. S27 – Comparison of time histories (forces) of NLFEDA modeling with laboratory results for FMRC(N)

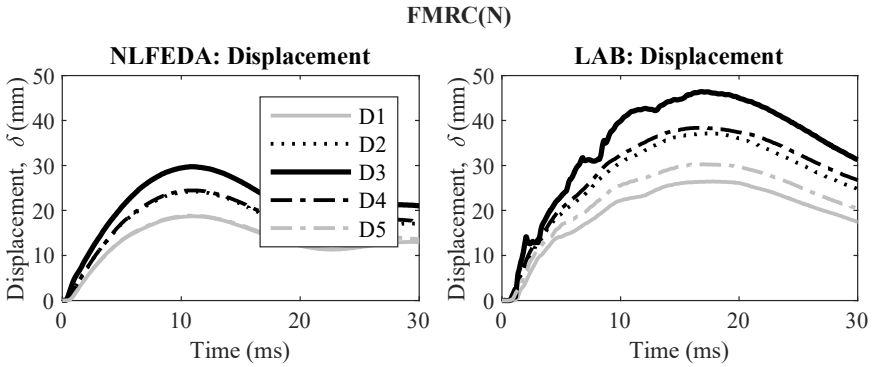

Fig. S28 – Comparison of displacement time histories of NLFEDA modeling with laboratory results for FMRC(N)

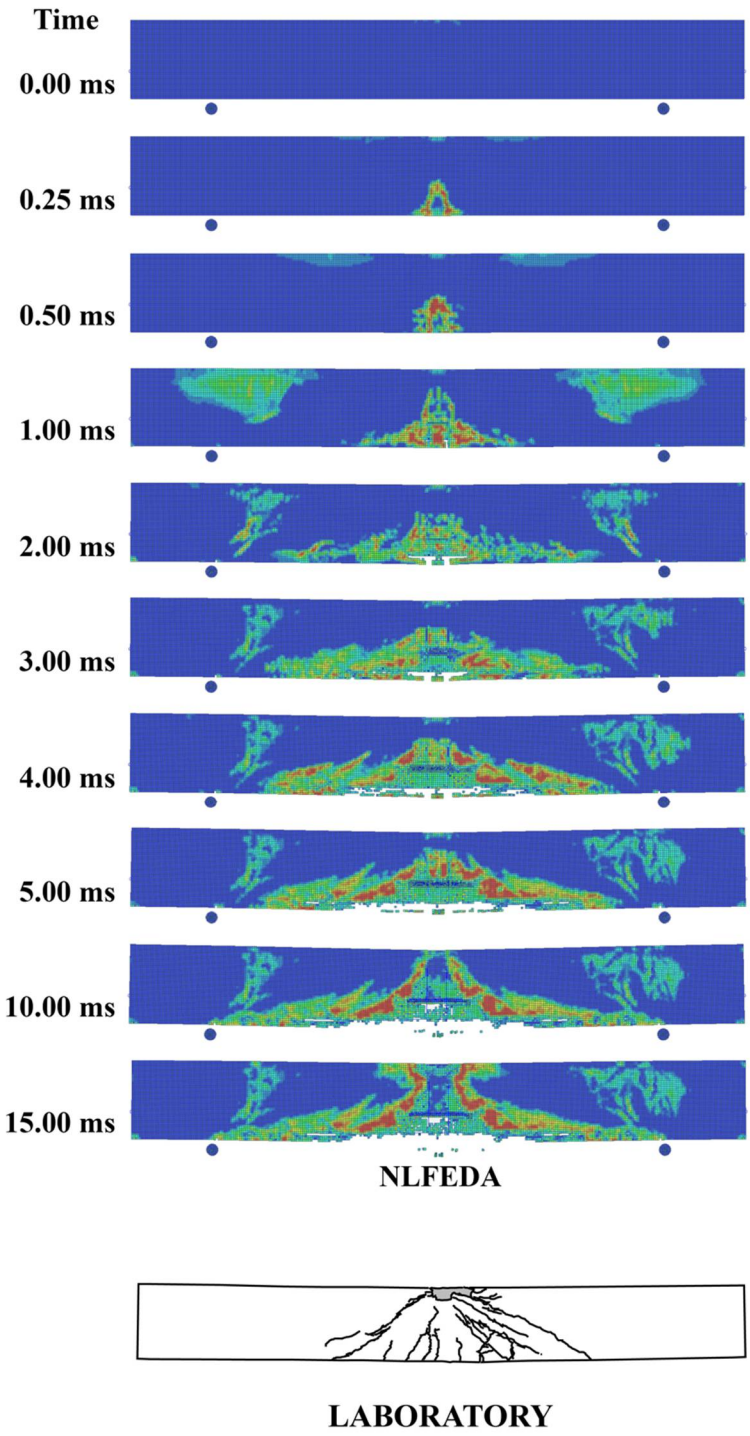

Fig. S29 – Progressive damage of FMPT0(N)

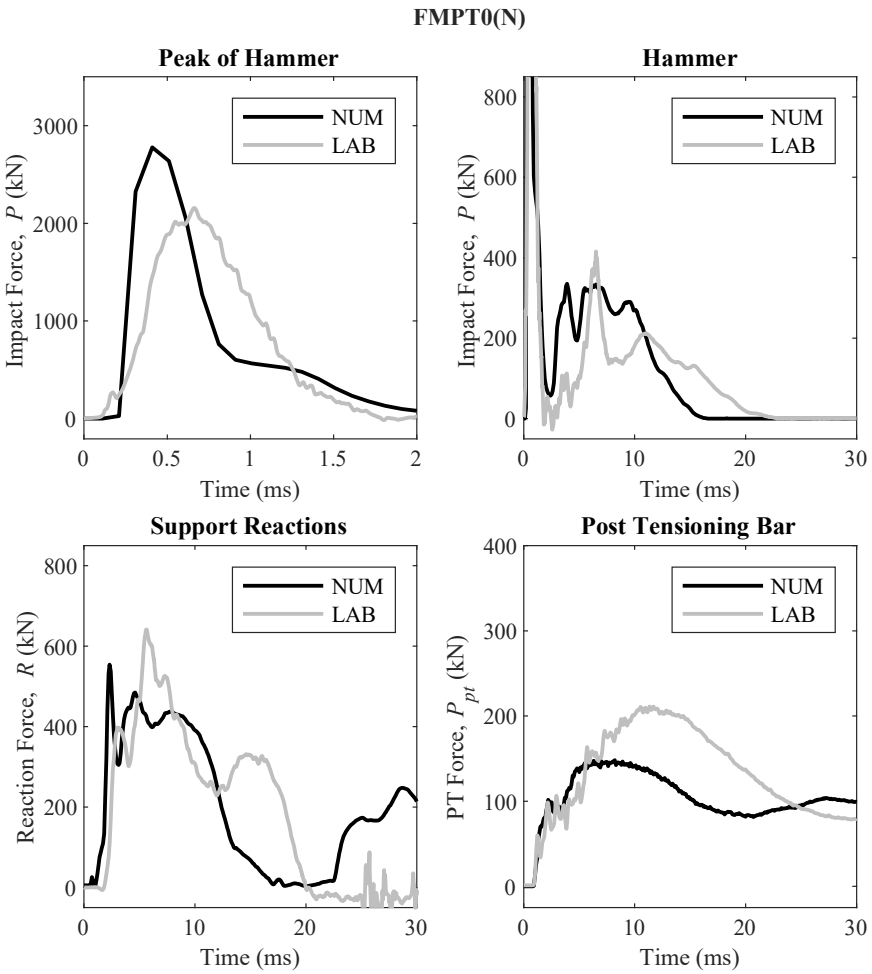

Fig. S30 – Comparison of time histories (forces) of NLFEDA modeling with laboratory results for FMPT0(N)

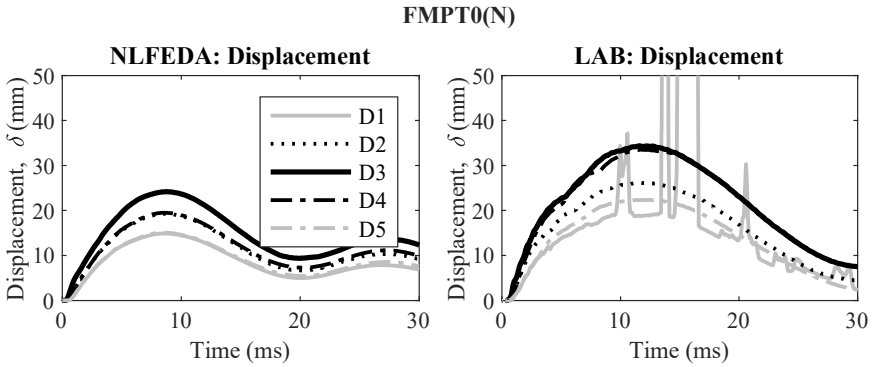

Fig. S31 – Comparison of displacement time histories of NLFEDA modeling with laboratory results for FMPT0(N)

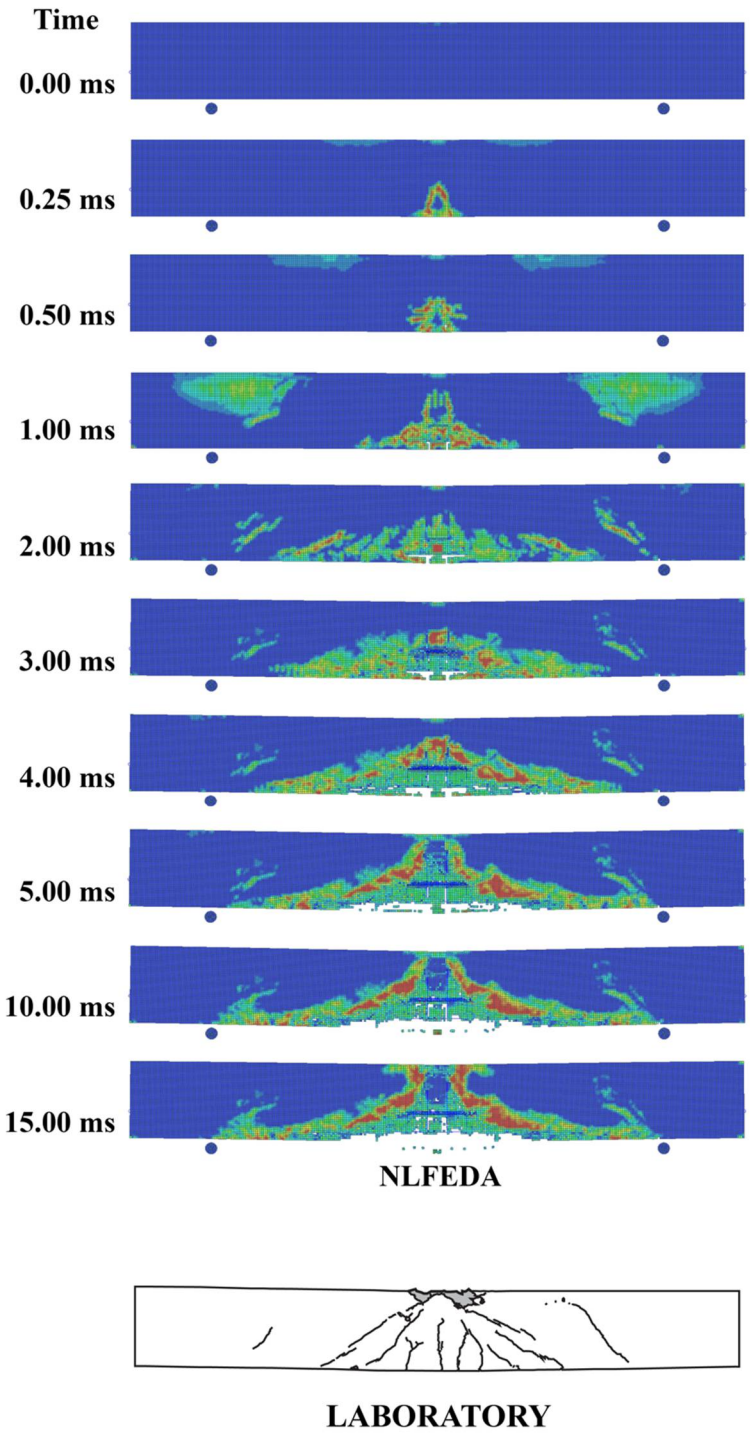

Fig. S32 – Progressive damage of FMPT60(N)

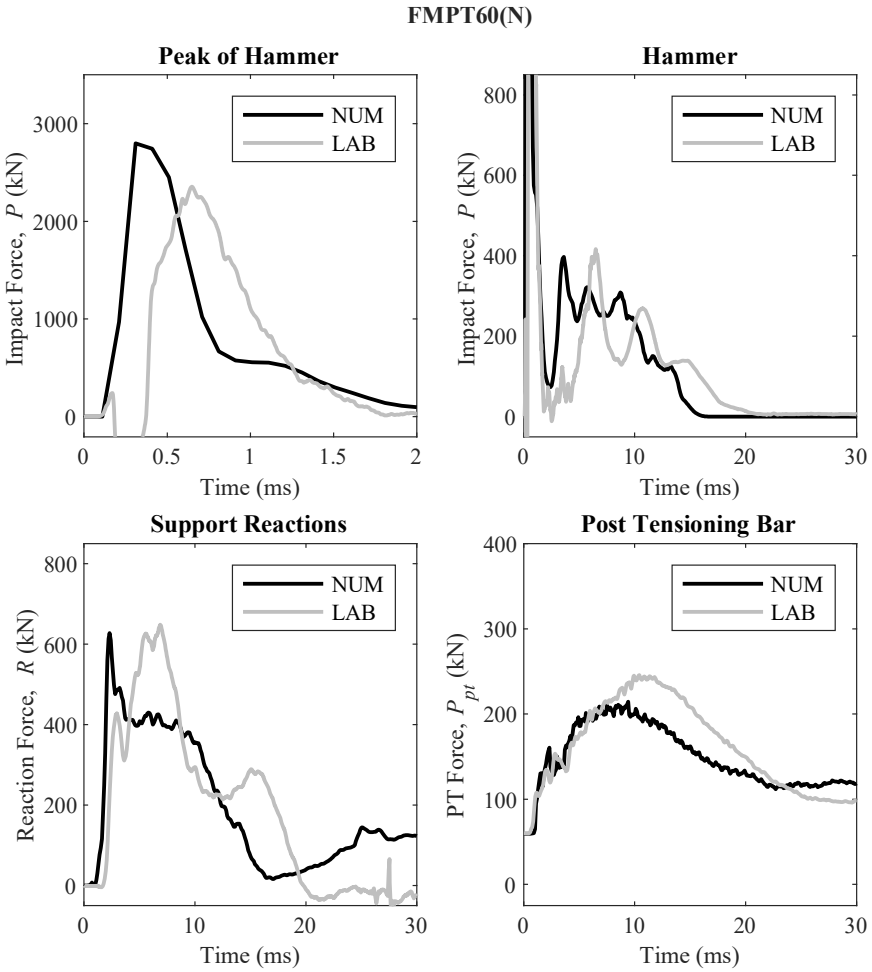

Fig. S33 – Comparison of time histories (forces) of NLFEDA modeling with laboratory results for FMPT60(N)

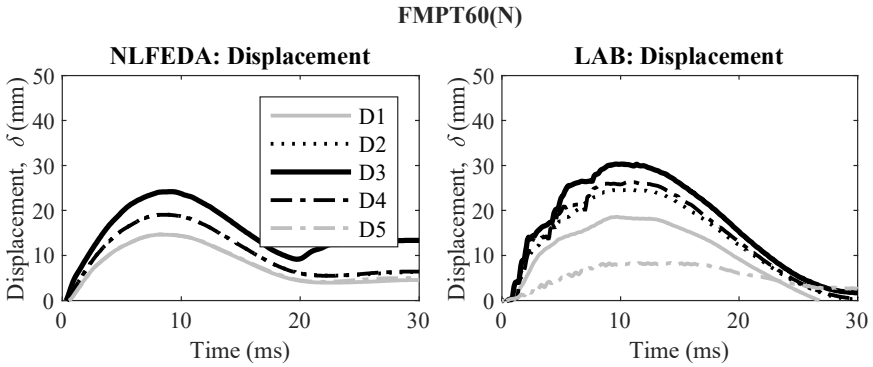

Fig. S34 – Comparison of displacement time histories of NLFEDA modeling with laboratory results for FMPT60(N)

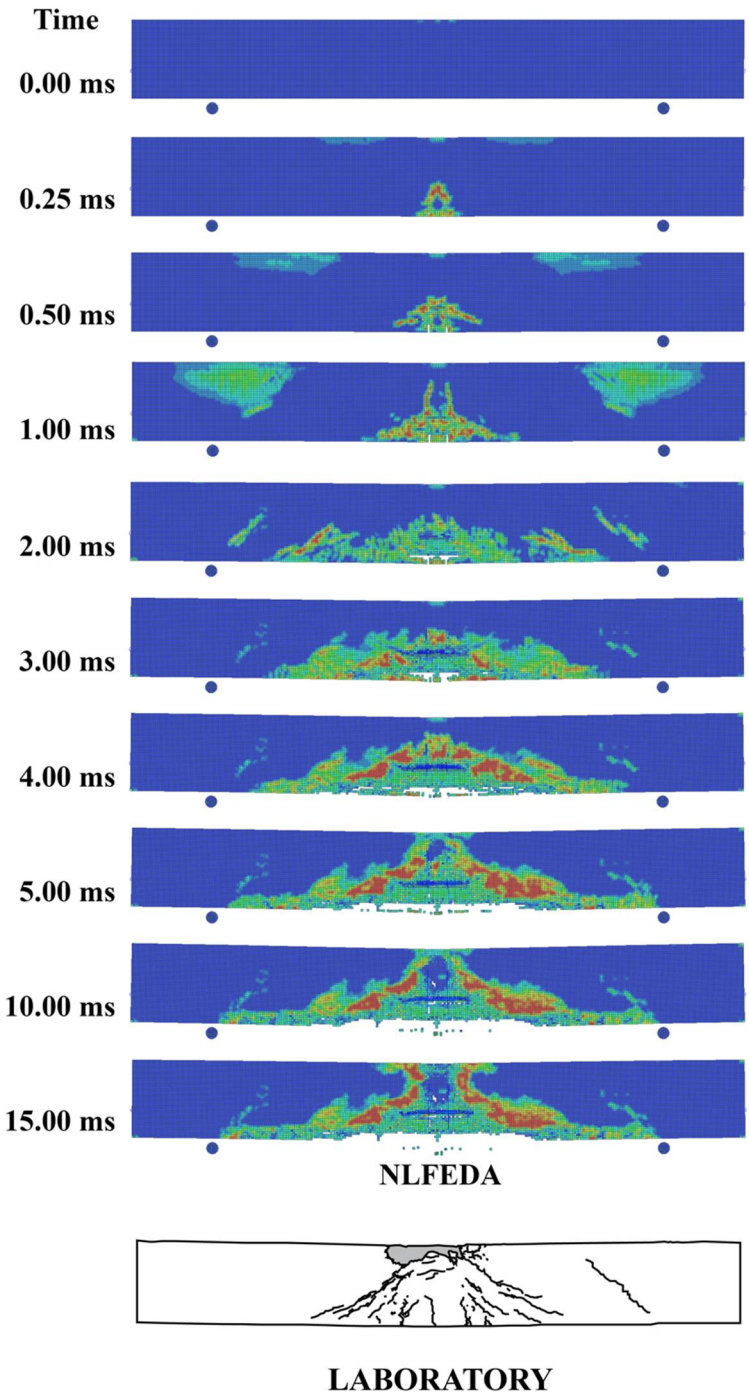

Fig. S35 – Progressive damage of FMPT109(N)

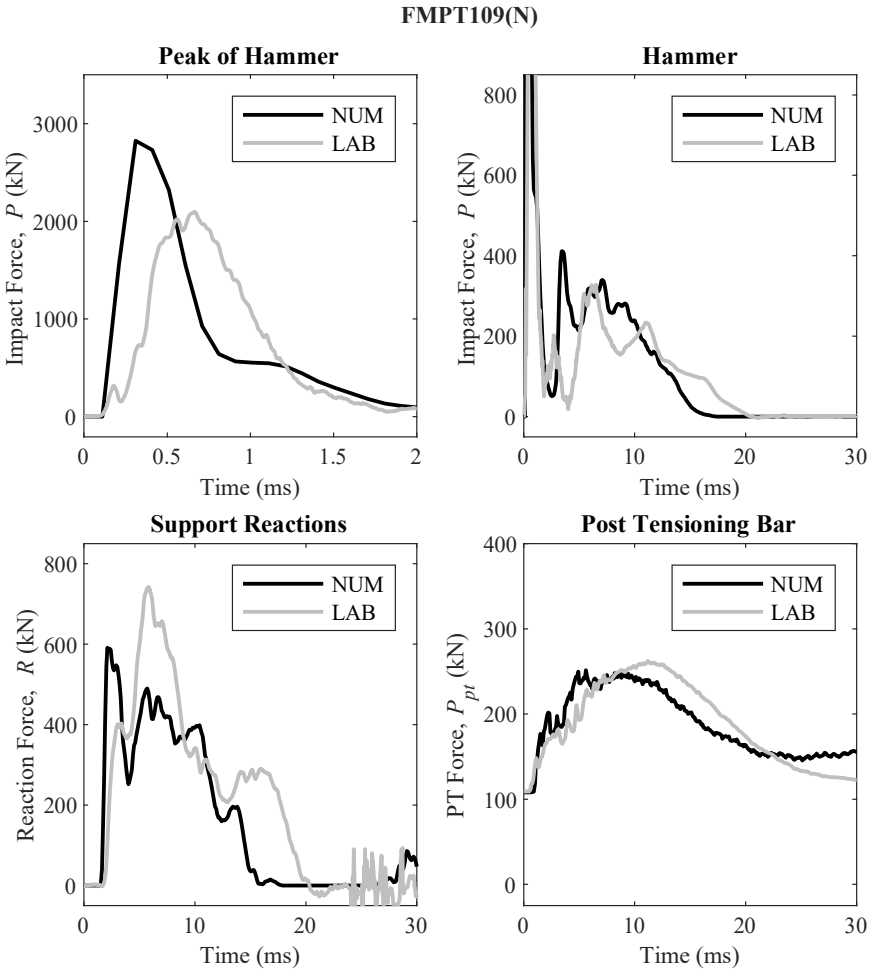

Fig. S36 – Comparison of time histories (forces) of NLFEDA modeling with laboratory results for FMPT109(N)

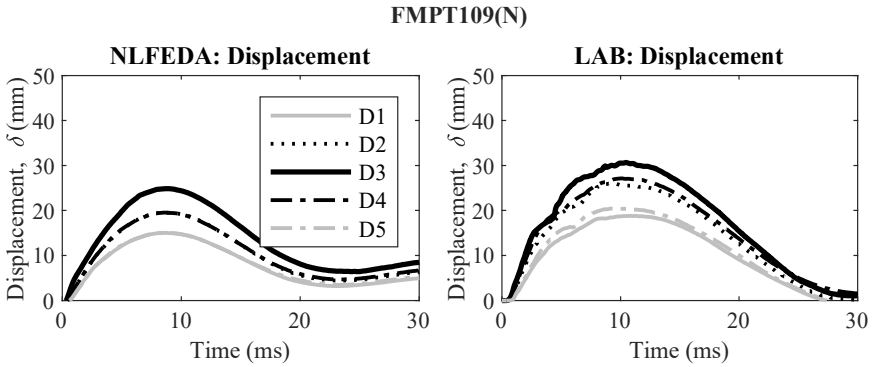

Fig. S37 – Comparison of displacement time histories of NLFEDA modeling with laboratory results for FMPT109(N)

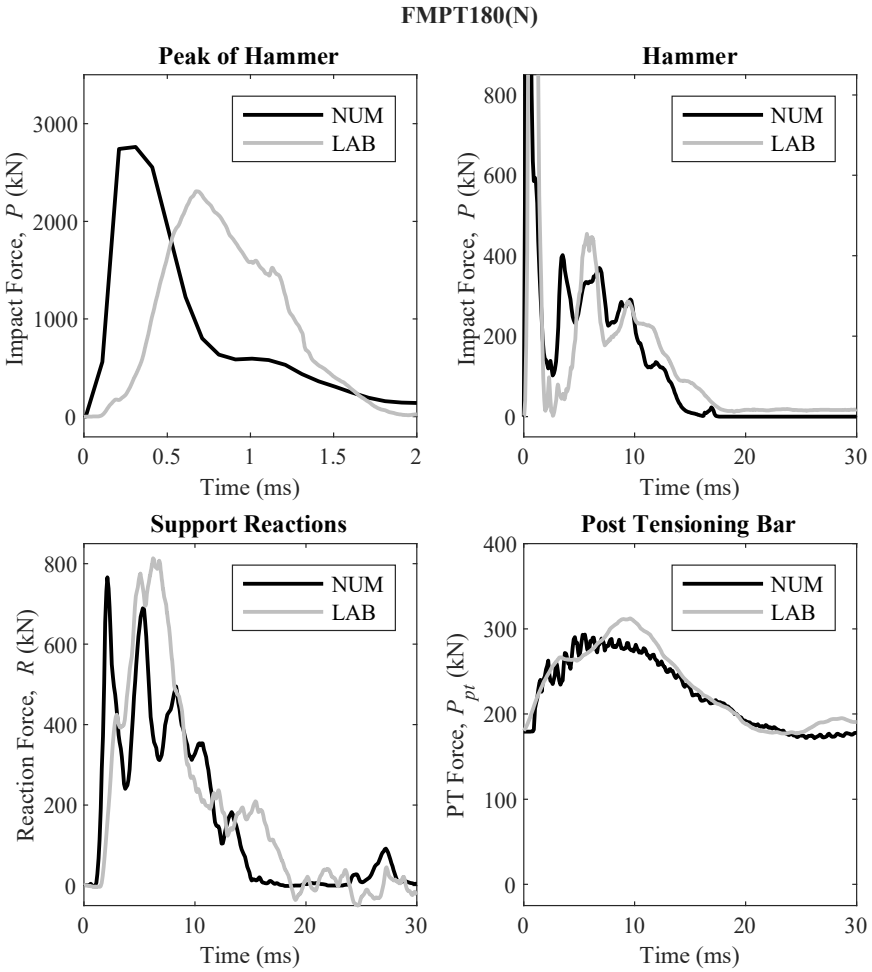

Fig. S38 – Comparison of time histories (forces) of NLFEDA modeling with laboratory results for FMPT180(N)

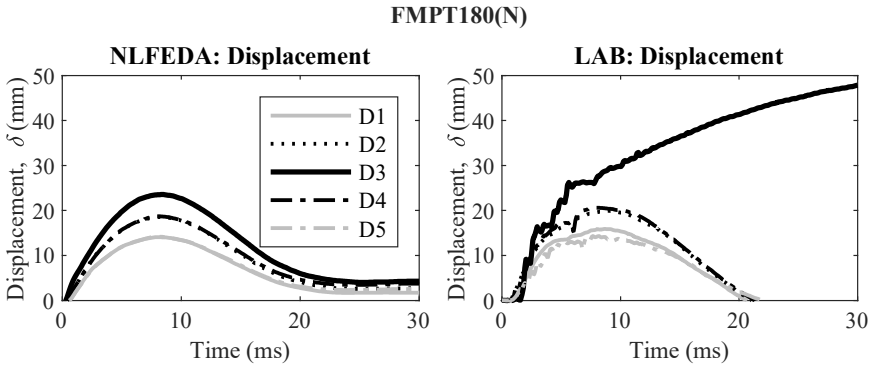

Fig. S39 – Comparison of displacement time histories of NLFEDA modeling with laboratory results for FMPT180(N)

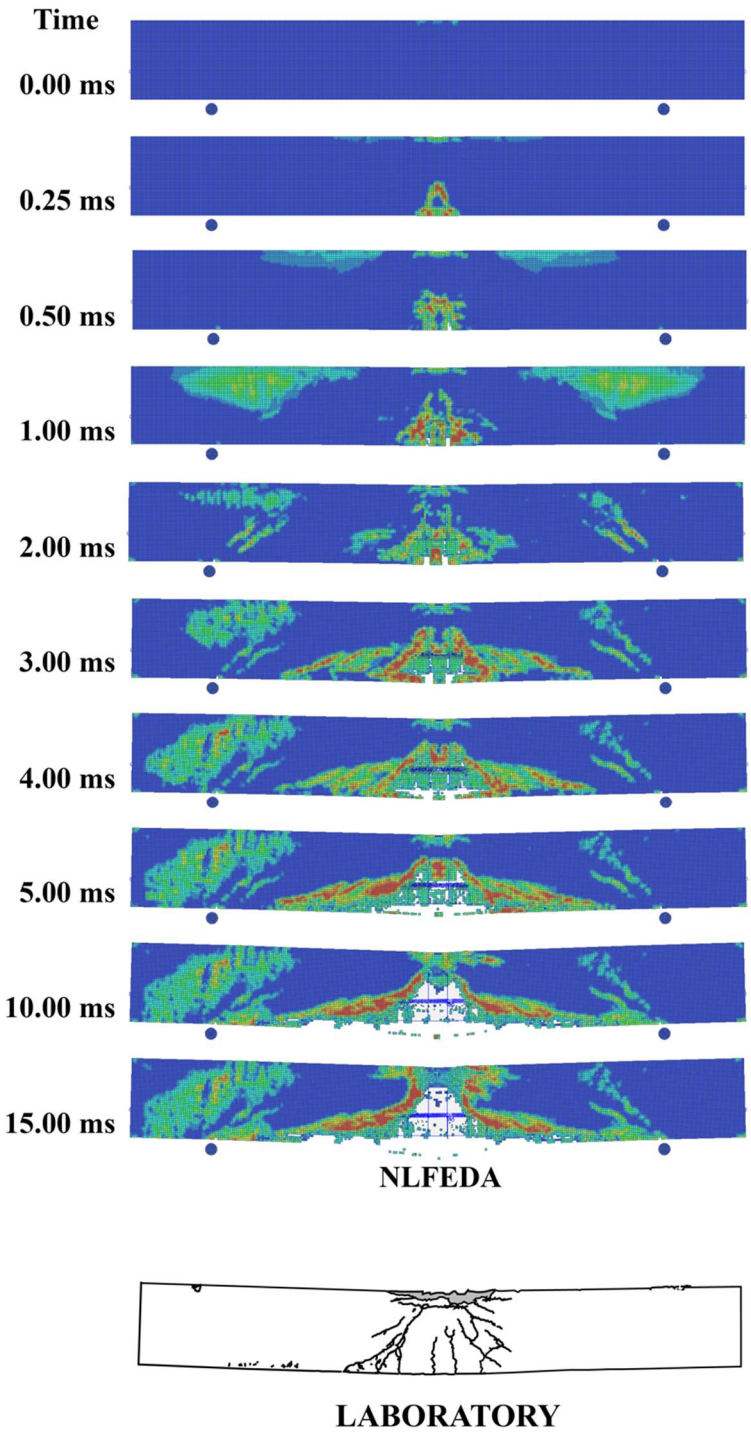

Fig. S40 – Progressive damage of FHPT0(N)

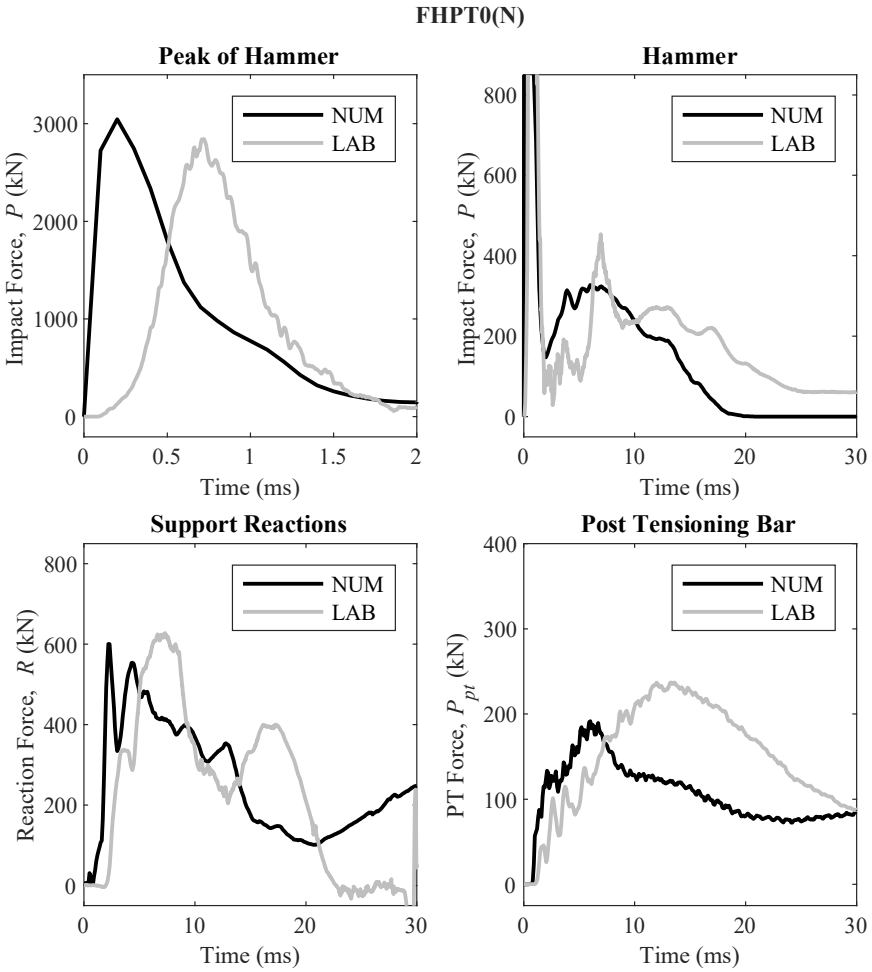

Fig. S41 – Comparison of time histories (forces) of NLFEDA modeling with laboratory results for FHPT0(N)

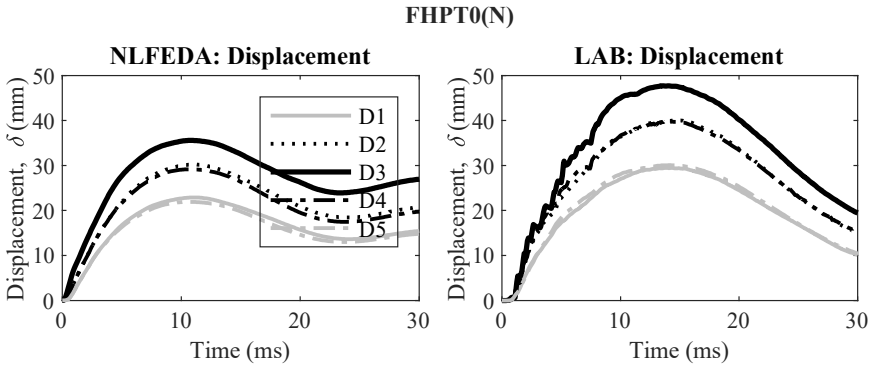

Fig. S42 – Comparison of displacement time histories of NLFEDA modeling with laboratory results for FHPT0(N)

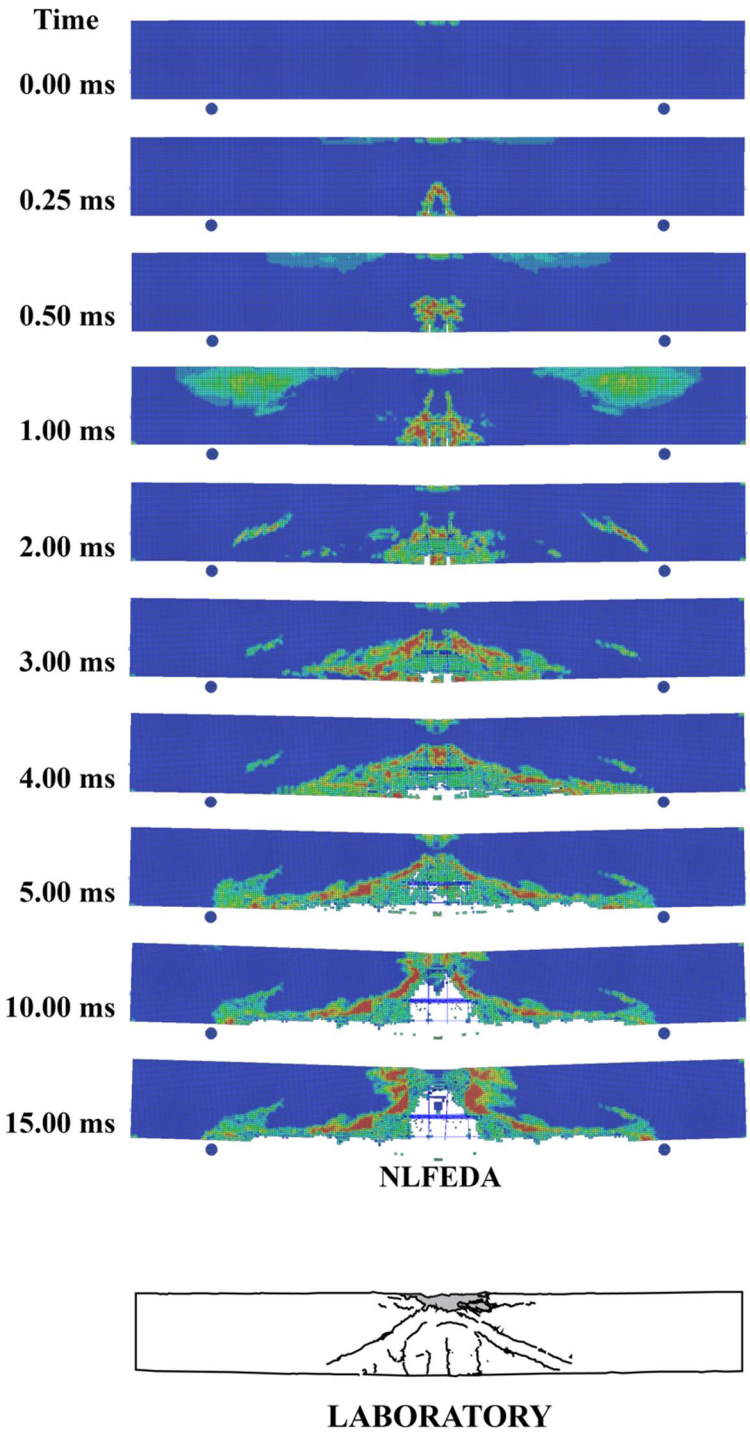

Fig. S43 – Progressive damage of FHPT122(N)

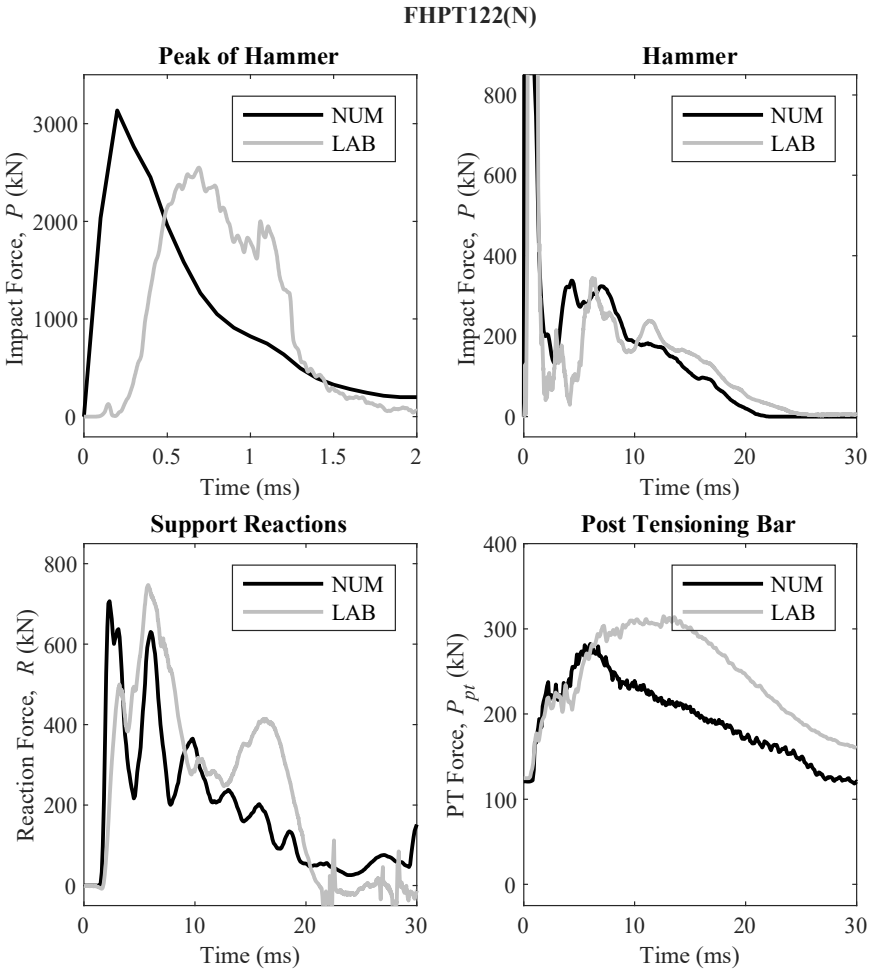

Fig. S44 – Comparison of time histories (forces) of NLFEDA modeling with laboratory results for FHPT122(N)

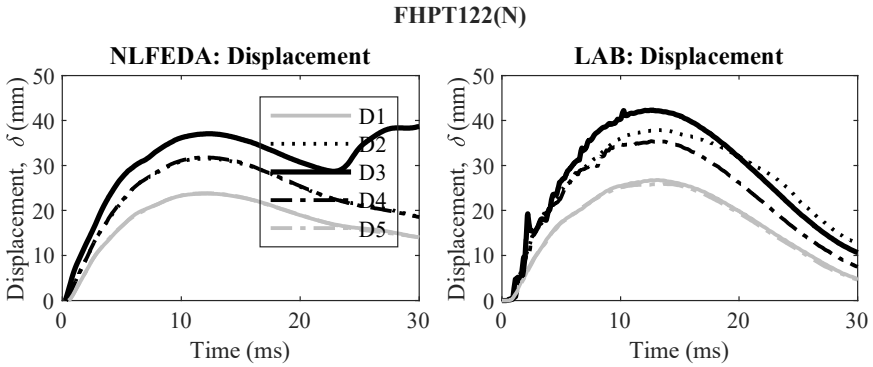

Fig. S45 – Comparison of displacement time histories of NLFEDA modeling with laboratory results for FHPT122(N)

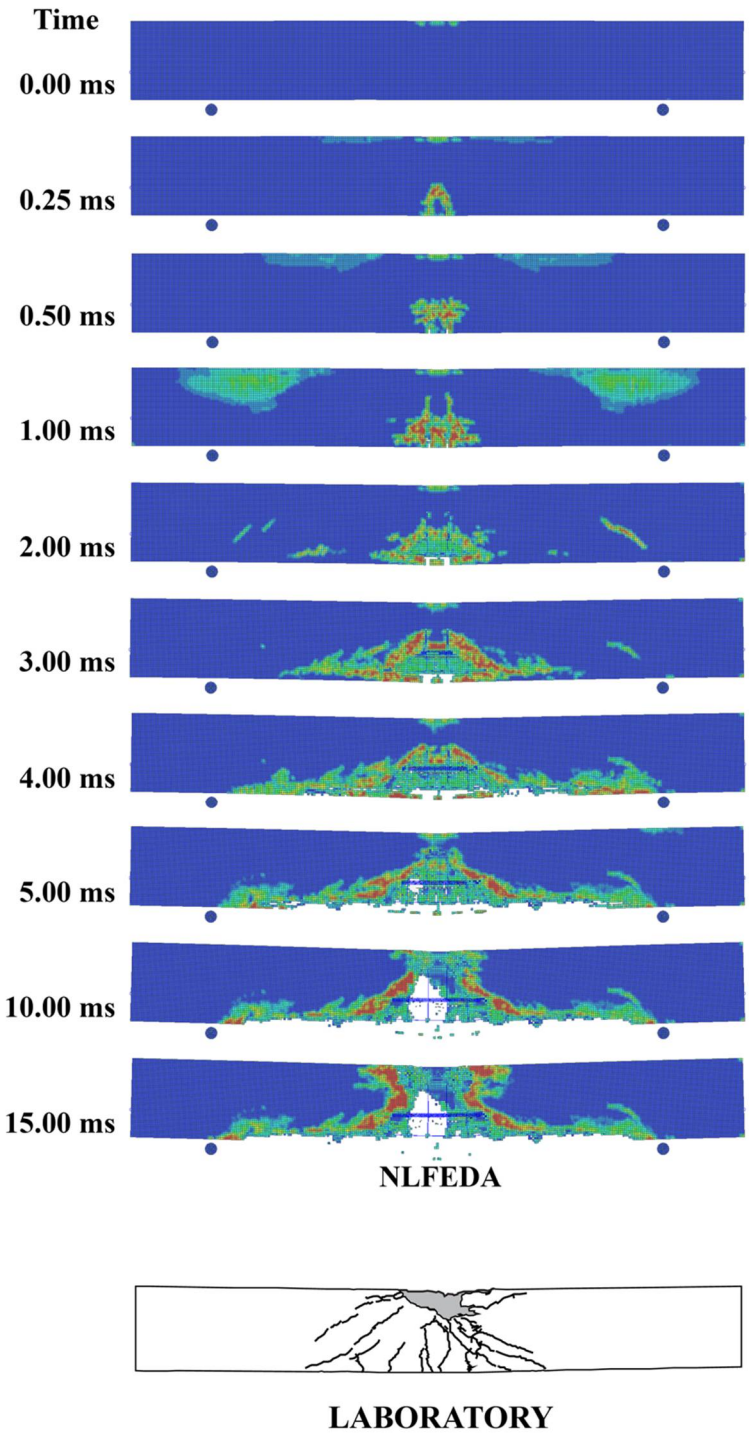

Fig. S46 – Progressive damage of FHPT200(N)

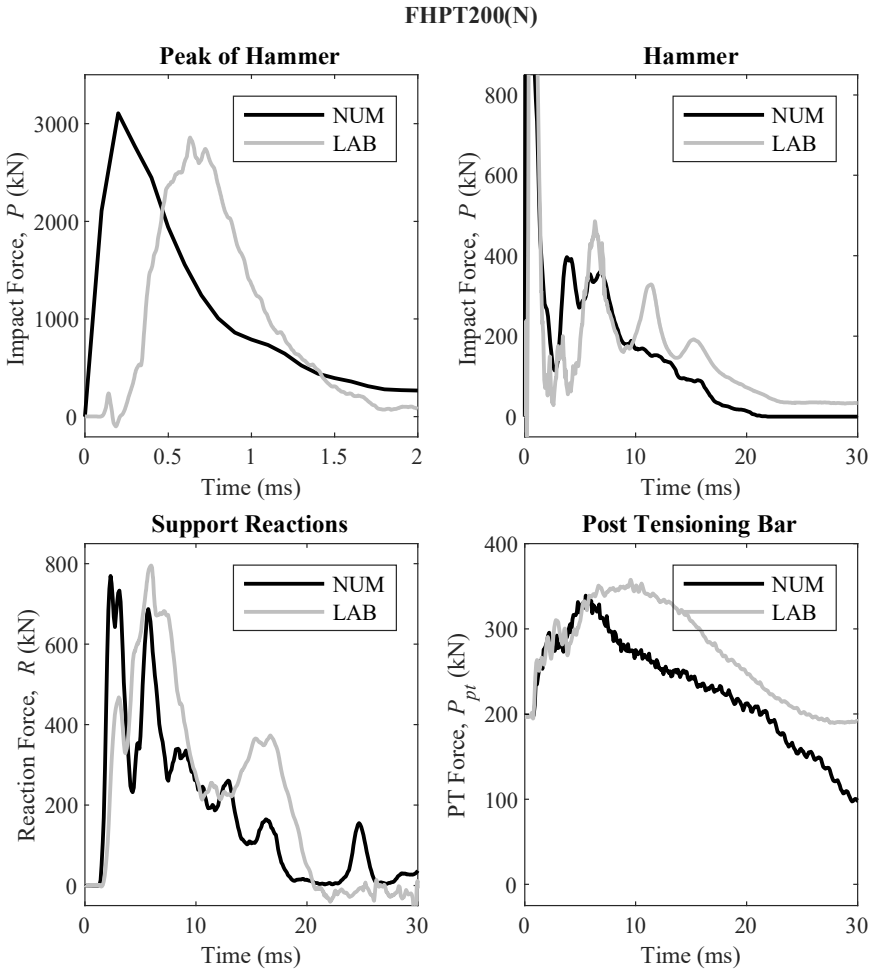

Fig. S47 – Comparison of time histories (forces) of NLFEDA modeling with laboratory results for FHPT200(N)

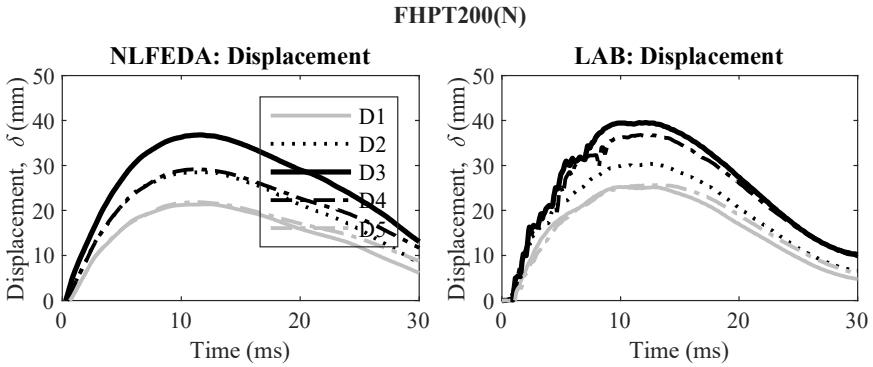

Fig. S48 – Comparison of displacement time histories of NLFEDA modeling with laboratory results for FHPT200(N)

Table S1 – Full testing matrix and parameters for experimental drop weight testing

ID	V_n (kN)	P_n (kN)	(V_n/P_n)	P_{pt_se} (kN)	f_{se} (Mpa)	H (m)	v (m/s)	E_k (kJ)
SLPT120	264	239	1.10	120	245	1.77	5.52	6.41
SLPT172	308	255	1.20	172	351	1.75	5.54	6.44
SMRC	120	159	0.76	NA	NA	3.50	7.90	13.11
SMPT0	163	183	0.92	0	0	3.52	8.35	14.64
SMPT57	211	213	1.00	57	116	3.51	8.46	15.04
SMPT118	262	239	1.09	118	240	3.54	8.00	13.44
SMPT170	306	255	1.20	170	346	3.52	7.98	13.36
FMRC	840	159	5.28	NA	NA	3.54	7.99	13.42
FMPT0	855	183	4.67	0	0	3.52	7.93	13.20
FMPT60	935	214	4.37	57	121	3.49	7.93	13.20
FMPT109	976	235	4.15	118	222	3.53	8.05	13.61
FMPT180	1036	258	4.02	170	367	3.50	8.25	14.31
FHPT0	855	159	5.38	0	0	5.19	10.73	24.17
FHPT122	987	241	4.10	122	248	5.25	11.04	25.63
FHPT200	1053	262	4.01	200	408	5.28	10.83	24.64